CODEN IEJMAT *Internet Electronic Journal of Molecular Design* **2005**, *4*, 279–308 ISSN 1538–6414
BioChem Press http://www.biochempress.com

Inter*net* Electronic Journal of Molecular Design

April 2005, Volume 4, Number 4, Pages 279–308

Editor: Ovidiu Ivanciuc

Proceedings of the Internet Electronic Conference of Molecular Design, IECMD 2003
November 23 – December 6, 2003

Avoided Curves Crossings of the Rydberg [$(AH_a^+)(e^-)_{Rydberg}$] (a = 2–4) Radical

Jong Keun Park

Department of Chemistry Education and Research Institute of Basic Science, Gyeongsang National University, Jinju 660–701, Korea

Received: November 14, 2003; Revised: July 21, 2004; Accepted: September 5, 2004; Published: April 30, 2005

Citation of the article:
J. K. Park, Avoided Curves Crossings of the Rydberg [$(AH_a^+)(e^-)_{Rydberg}$] (a = 2–4) Radical, *Internet Electron. J. Mol. Des.* **2005**, *4*, 279–308, http://www.biochempress.com.

Inter*net* Electronic Journal of Molecular Design

BioChem Press
http://www.biochempress.com

Avoided Curves Crossings of the Rydberg $[(AH_a^+)(e^-)_{Rydberg}]$ (a = 2–4) Radical [#]

Jong Keun Park *

Department of Chemistry Education and Research Institute of Basic Science, Gyeongsang National University, Jinju 660–701, Korea

Received: November 14, 2003; Revised: July 21, 2004; Accepted: September 5, 2004; Published: April 30, 2005

Internet Electron. J. Mol. Des. **2005**, *4* (4), 279–308

Abstract

Potential energy curves of the ground and low lying excited states for the dissociation of the Rydberg AH_a (NH_4, H_3O, H_2F; 11 electron species) radical into [AH_b + H_c; b = 1–3, c=1–2, b+c = a] have been calculated using *ab initio* Hartree–Fock (HF) and singly and doubly excited configuration interaction (SDCI) methods with a large basis set including Rydberg basis functions. In the ground and excited correlation curves, the potential curves of the $[(AH_a^+)(e^-)_{Rydberg}]$ radical diabatically correlate to the [AH_b (n→3s, 3p) + H_c] and the [AH_b^+ + H_c^-] asymptotes. At shorter than $R_{(AH)} \cong 2.0$ Å, the avoided curve crossings between the dissociative diabatic states of the $[(AH_a^+)(e^-)_{Rydberg}]$ radical and the repulsive diabatic states emerging from the antibonding interactions of the [AH_b (n→3s, 3p) + H_c] asymptotes are found mainly. While, at larger than $R_{(AH)} \cong 2.0$ Å, the avoided curve crossings between the attractive diabatic states emerging from a bonding interaction of the [AH_b^+ + H_c^-] asymptotes and the repulsive diabatic states from the antibonding orbitals of its asymptotes are found. A maximum position of the potential energy barrier of the ground correlation curve is located out of line of those of the excited states. The potential energy barriers formed by some avoided curve crossings are found to be relatively low. The potential wells are shallowly quasibound. The potential energy gaps between the Rydberg AH_a radical and its dissociation asymptotes are very low. The relative stabilities of metastable states from NH_4 to H_2F are decrease monotonously.

Keywords. Rydberg radical; potential energy curve; avoided curve crossing; diabatic state; adiabatic state; asymptote; metastable state; configuration interaction; potential well; potential energy gap.

Abbreviations and notations

CCSD(t), coupled cluster with both single and double substitution	MP2, second–order Möller–Plesset
CI, configuration interaction	MRD–CI, multireference double configuration interaction
CIPSI, equivalent to a multireference Möller–Plesset second order method	ROHF, restricted open Hartree–Fock
HF, Hartree–Fock	SDCI, singly and doubly excited configuration interaction
	UHF, unrestricted Hartree–Fock
	UHF–CI, unrestricted Hartree–Fock configuration interaction

[#] Presented in part at the Internet Electronic Conference of Molecular Design, IECMD 2003.

* Correspondence author; E–mail: mc7@nongae.gsnu.ac.kr.

1 INTRODUCTION

Recently, the photodissociation reactions of the Rydberg [$(AH_a^+)(e^-)_{Rydberg}$] radical have been one of the issues as a fundamental unit in photochemical processes of $(AH_{a-1})_n$ clusters [1–64]. Since the [$(AH_a^+)(e^-)_{Rydberg}$] radical has a short lifetime and a low energy barrier relative to the corresponding dissociative products [$(AH_{a-1} + H)$, $(AH_{a-2} + H_2)$], the stabilities and electronic structures of AH_a have been widely characterized by experimental [1–19,33–42,63,64] and theoretical [20–32,43–62] methods. The AH_a radical in clusters has been known to be stabilized by the complexation with its neutral molecule species [1–19,33–42]. For example, the lifetime of the NH_4 radical in ammonia clusters [1–7] was observed to be 10^6 times longer than that of the monomer. The lifetime of NH_4 is shorter than 1 μs, while those of ND_4 and NT_4 are longer than 10 μs. NH_4 relative to its dissociation products is unstable by 1.1 kcal/mol, while ND_4 and NT_4 are stable by 0.5–1.2 kcal/mol. Because of the slightly high dissociation barriers of the isotopic species (ND_4, NT_4), the stabilities of these species in stead of NH_4 have been studied extensively [8–19]. The stability and existence of the Rydberg H_3O radical have been one of the topics in the quantum dynamics and energetics of $(H_2O)_n$ clusters [33–51]. The Rydberg $(H_3O^+)(e^-)_{3s}$ radical can be stabilized by the complexation with water species like a Rydberg $(NH_4^+)(e^-)_{3s}$ radical.

Since the stabilities and Rydberg transitions of NH_4 firstly suggested by Schuster [8] and Schüler *et al*. [9], the existence of the NH_4 radical have been characterized by various theoretical methods [20–32]. According to the potential energy curves of NH_4 constructed by Kassab and Evleth [21,22], the stability and electronic structure of NH_4 depend on its structural correlation with the first Rydberg excited state emerging from $(NH_3 + H)$ and $(NH_2 + H_2)$. The potential energy barrier of the state is made from the avoided curve crossing between the dissociative state of $(NH_4^+)(e^-)_{3s}$ and the repulsive state emerging from $(NH_3 + H)$ and $(NH_2 + H_2)$. The potential barriers and dissociation products are found to be high by some electron volts. By the potential energy curves of Kaspar *et al*. [23], the relative stability and the dissociation barrier were depended by the electron correlation. At the UHF level, the dissociations of NH_4 into $(NH_3 + H)$ or $(NH_2 + H_2)$ are both exothermic, while, at the SDCI level, the dissociations are endothermic. According to the potential energy curves of Cardy *et al*. [25], the formation reaction of NH_4 from $(NH_2 + H_2)$ is slightly exothermic, whereas the reaction from $(NH_3 + H)$ is endothermic. By the above results, the lifetime of NH_4 is essentially depended on the height of the potential energy barrier for the dissociation of NH_4 into its asymptotes.

Since the existence of H_3O based on thermodynamic cycles are firstly suggested by Bernstein [33], the stabilities of the Rydberg H_3O radical have been performed by various experimental techniques [34–42]. By indirect kinetic studies, the existence of H_3O as an intermediate (a lifetime of $\cong 10^{-10}$ sec) of the radiolysis of water was reported by Magee [34], Sworski [35], and Kongshang *et al*. [36]. Using mass spectrometer equipped with two different reactors designed to produce

reactive species, Melton and Joy [37] detected the existence of the H_3O species produced by irradiating water vapor with ionizing electron. Martin and Swift [38] claimed to have obtained the ESR spectrum of H_3O. Gellene and Porter [40] generated the oxonium H_3O radical by neutralizing a fast beam of ions in the near resonant electron transfer reaction. But, some workers could not obtain any experimental results for the existence of H_3O. In the collisions of beam of H and H_2O conducted by Bassi *et al*. [42], any evidence for a bound state in the relative velocity range of $\cong 10^{-5}$ (cm/sec) was not investigated. In ion–beam study performed by Williams and Porter [10], a metastable state of H_3O with a lifetime greater than 10^{-7} sec was not obtained.

The stabilities of H_3O and the ground potential energy curve of the dissociation of H_3O into (H_2O + H) or (OH + H_2) have been theoretically investigated by some groups [37,43–51]. Melton and Joy [37], Bishop [43], and Schwarz [50] groups suggested that the stability of H_3O would be stable or metastable relative to its asymptotes. According to their curves investigated by Gangi and Bader [44], Niblaeus *et al*. [46], and Luo and Jungen [49], the ground $^2A_1$ state surface along the OH bond rupture has a very low energy barrier and the curve is quasibound state. Gangi and Bader studied the ground potential energy curve for the dissociation reaction of H_3O into (H_2O + H) using the UHF method. At $R_{(OH)} \cong 1.21$ Å, the energy barrier of the dissociation reactions is found to be $\cong 0.29$ eV. The dissociation energy and vertical ionization energy are $\cong$ 1.22 and $\cong$ 5.36 eV, respectively. Using an UHF–CI method, the energy surface of H_3O is performed by Niblaeus *et al*. At $R_{(OH)} \cong 1.248$ Å, the potential barrier is found to be $\cong 0.13$ eV. The energy gap between H_3O and (H_2O + H) is $\cong$ 0.89 eV. In the various possible dissociation paths of H_3O into (H_2O + H) investigated by Luo and Jungen, the ground potential energy curve ($^2A_1$) along the OH bond rupture has a very low barrier of $\cong$ 0.08 eV. The curve is quasibound state. At $R_{(OH)} \cong 2.5$ Å, the curve is also bound shallowly. But, Lathan *et al*. [45] claimed that H_3O would be unstable with respective to its asymptotes. They concluded that the origin of the barrier is an avoided curve crossing between a repulsive state and an attractive Rydberg state. The barrier height of the curve is investigated to be relatively low. And the formation reaction of AH_a from its dissociation products are isoenergetic or very slightly endothermic [20–32,43–51]. But, the avoided curve crossings have not been represented clearly.

The stabilities and electronic structures of H_2F with bent or linear geometry have been studied with the various theoretical [52–62] and experimental [63,64] methods. H_2F with 11 electron systems is isoelectronic structure with NH_4 and H_3O, which are observed in the metastable states. By a combination of neutralized ion beam and charge stripping techniques [63], an experimental evidence for metastable state of D_2F is observed by Raksit *et al*. The lifetime of the metastable state is greater than 0.4 μs. But, the metastable states of HDF or H_2F are not observed. Using the MRD–CI method, the ground and few excited states of H_2F were calculated by Petsalakis *et al*. [58]. These states are bound and have potential minima at the geometry similar to that of the cation H_2F^+. Until now, except for the result of Petsalakis *et al*., the metastable state of H_2F have not been found [52–

57,59–64].

Although the stabilities and geometric structures of [$(AH_a^+)(e^-)_{Rydberg}$] in the hydrated and neutral molecule clusters have been studied with the various methods, the investigation of the potential energy curves for the dissociation of [$(AH_a^+)(e^-)_{Rydberg}$] into (AH_b + H_c) seems to be worth carrying out on the basis of the following points. (*i*) How are relative potential barriers of the potential energy curves for dissociation reactions from NH_4 to H_2F? (*ii*) On the ground and low lying excited curves, a maximum position is represented between $R_{(AH)} \cong$ 1.5 and 2.5 Å, while, on the highly excited curves, two maximum positions are represented. What kinds of avoided curve crossings are occurred on the dissociation reactions? (*iii*) Why is the maximum position made by the avoided curve crossing located near the equilibrium geometry ($R_{(AH)} \cong$ 1.59 and 1.40 Å)? (*iv*) Is the barrier height of the ground potential curve found to be low or high? (*v*) Is the dissociation reaction of AH_a into (AH_b + H_c) endothermic or exothermic? (*vi*) The potential energy barriers of the potential curves for the dissociation reaction of AH_a into (AH_b + H_c) are not yet investigated clearly. Are the energy barriers of the potential curves made by the avoided curve crossing? To answer above questions, we have studied the state–to–state correlation curves for AH_a dissociating into (AH_b + H_c) in order to investigate the stabilities and avoided crossings. Our correlation curves give the detailed informations of the crossing positions and barrier heights for AH_a dissociating into (AH_b + H_c).

2 COMPUTATIONAL METHODS

The basis sets chosen are the triple zeta basis on N (521/2111) [65], O (5311111/32111) [66], and H(511) [67]. Two extra d type polarization functions are added to nitrogen (α_d = 0.412, 1.986) [65] and oxygen (α_d = 2.22, 0.874) [68]. One extra p type function is added to hydrogen (α_p = 0.990495) [65]. The diffuse Rydberg basis functions are additionally augmented on nitrogen (α_s = 0.028, 0.0066; α_p = 0.025, 0.0051; α_d = 0.015, 0.0032) [69] and oxygen (α_s = 0.008, 0.032; α_p = 0.051, 0.02; α_d = 0.345, 0.143) [68] to describe the Rydberg states of NH_2, NH_3, NH_4, H_2O, and H_3O. Descriptions of chemical compounds, chemical databases, software, and algorithms should be given in detail to enable qualified scientists to reproduce the results.

To draw the potential energy curves, we have used the characteristics of the states twofold. For the dissociation of AH_a into its dissociation products, the molecular orbital and geometric structure at each internuclear distance are calculated with the restricted open shell Hartree–Fock method (ROHF). And the molecular orbital and optimized structure were used as input for subsequent the singly and doubly excited configuration interaction (SDCI) calculation. That is, the molecular orbital for a configuration interaction (CI) is determined with ROHF's result. The singly and doubly excited configuration interaction method is used for the potential energy calculation with the GAMESS package. By changing the internuclear distance, the whole procedure has been repeated

from AH_a to its dissociation products. The internuclear distances [$R_{(AH)}$] range are from 0.9 to 14.0 Å. The SDCIs for the neutral (H_2, NH_2, NH_3, NH_4, OH, H_2O, and H_3O) and ionic species (H^-, H_2^-, NH_2^+, NH_3^+, OH^+, H_2O^+, and H_3O^+) are also performed separately.

Table 1. Bond lengths (Å) and relative energies (eV) for the NH_4 radical dissociating into (NH_3 + H) and (NH_2 + H_2). Ionization and excitation energies (eV) of NH_4, NH_3, and NH_2. The numbers in parentheses indicate the vertical ionization energy

	SECI[a]	SDCI[a]	MP2[b]	CCSD(t)[b]	CIPSI[c]	SDCI[d]	exptl[e]
$^2A_1$ state emerging from (NH_3 + H)							
$R_{(NH)eq}$	1.022	1.040	1.034	1.040	1.033	1.041	
$R_{(NH)TS}$	1.339	1.439	1.411	1.425	1.369	1.427	
$\Delta E_{(NH4–TS)}$	0.75	0.83	0.77	0.79	0.88	0.85	
$\Delta E_{[TS–(NH3+H)]}$	0.59	0.61	0.60	0.57	0.52	0.64	
$\Delta E_{[NH4–(NH3+H)]}$	–0.17	–0.22	–0.20	–0.22	–0.23	–0.21	–0.3
$^2A_1$ state emerging from (NH_2 + H_2)							
$R_{(NH)eq}$		1.039	1.036	1.040	1.033	1.041	
$R_{(NH)TS}$		1.590					
$\Delta E_{(TS–NH4)}$		3.59					
$\Delta E_{[TS–(NH2+H2)]}$		1.06					
$\Delta E_{[NH4–(NH2+H2)]}$		–2.53					
$^2B_1$ state emerging from (NH_2 + H_2)							
ΔE_{eq}		1.015					
ΔE_{TS}		1.590					
$\Delta E_{(TS–NH4)}$		2.96					
$\Delta E_{[TS–(NH2+H2)]}$		4.66					
$\Delta E_{[NH4–(NH2+H2)]}$		–1.69					0.32
NH_4							
I.E.[f]	4.52	4.57	4.58	4.60		4.85[g]	4.62[h], 4.73[i]
$\Delta E_{(3s–3p)}$	1.55	1.90			1.66	1.89	
$\Delta E_{(3s–4s)}$	2.46	2.66			2.65		
$\Delta E_{(3s–3d)}$; $^2T_2$	2.61	2.85				2.89	2.19[j]
$\Delta E_{(3s–3d)}$; ^2E	2.69	2.93				3.04	
$\Delta E_{(3s–4p)}$	2.90	3.15					
$\Delta E_{(3s–5s)}$	3.22	3.45					
$\Delta E_{(3s–4d)}$; $^2T_2$	3.29	3.53					
$\Delta E_{(3s–4d)}$; ^2E	3.32	3.61					
$\Delta E_{(3p–3d)}$; $^2T_2$	1.06	1.23					1.87[j]
NH_3							
I.E.[f]	10.02	10.13	10.10	10.14			10.17[l]
P.A.[k]	9.18	9.22	9.23	9.24	9.58[m]	9.23[n]	
$\Delta E_{(n–3s)}$; A^3A_1	6.46	6.31				6.27[o]	6.38[l]
$\Delta E_{(n–3px,y)}$; B^3E	7.88	7.86				7.84[o]	7.90[l]
$\Delta E_{(n–3pz)}$; $^3A_1$	8.29	8.05				7.84[o]	8.14[l]
$\Delta E_{(n–4s)}$; $^3A_1$	8.98	9.06					9.11[l]
$\Delta E_{(n–3d)}$; ^3E	9.09	9.23					

Table 1. (Continued)

	SECI[a]	SDCI[a]	MP2[b]	CCSD(t)[b]	CIPSI[c]	SDCI[d]	exptl[e]
NH_2							
I.E.[p]		11.0(11.77)[r]		11.20[s](11.37)[t]	10.9[u]	11.14[v]	11.46(12.00)[t]
I.E.[q]		12.16(12.22)[r]		12.48[s](12.10)[t]		12.45[v]	12.45(12.45)[t]
$\Delta E_{(12B1-12A1)}$	2.22	2.20[w]			2.26[y]	2.16[z]	
$\Delta E_{(12B1-12B2)}$	6.58	6.50[w]			6.50[y]	6.64[z]	
$\Delta E_{(12B1-22A1)}$	7.59	7.55[w]		7.74[x]	7.77[y]	7.69[z]	
$\Delta E_{(12B1-22B1)}$	7.65	7.62[w]		7.70[x]	7.49[y]	7.63[z]	
$\Delta E_{(12B1-32B1)}$	9.46	9.38[w]		9.45[x]	9.57[y]	9.46[z]	
$\Delta E_{(12B1-42B1)}$	9.69	9.43[w]		9.76[x]			
$\Delta E_{(12B1-32A1)}$	9.80	9.61[w]		10.06[x]			
$\Delta E_{(12B1-52B1)}$	9.87	9.83[w]		9.83[x]			
$\Delta E_{(12B1-42A1)}$	9.90	9.87[w]		9.89[x]			
$\Delta E_{(12B1-62B1)}$	10.29	10.18[w]		10.08[x]			
$\Delta E_{(12B1-52A1)}$	10.48	10.46[w]		11.51[x]			
$\Delta E_{(12B1-72B1)}$	11.64	11.49[w]		11.42[x]			
$\Delta E_{(12B1-62A1)}$	11.68	11.59[w]					
$\Delta E_{(12B1-72A1)}$	12.17	12.21[w]					

[a] SECI and SDCI energies were obtained with the MOs and geometries of NH_4^+ calculated by RHF at each internuclear distance. [b] CCSD(t) energies were obtained with Gaussian 98. [c] Reference [22]. [d] Reference [23]. [e] Cited from reference [22]. [f] Ionization energies of NH_4 and NH_3. [g] Reference [27]. [h] Reference [4]. [i] Reference [11]. [j] Reference [5]. [k] Proton affinity of NH_3. [l] Reference [70]. [m] Reference [30]. [n] Reference [71]. [o] Reference [72]. [p] Adiabatic ionization energy of X^3B_1 of NH_2^+ from X^2A_1 of NH_2. [q] Adiabatic ionization energy of A^1A_1 of NH_2^+ from X^2A_1 of NH_2. [r] Reference [73]. [s] Reference [74]. [t] Reference [75]. [u] Reference [76]. [v] Reference [77]. [w] Reference [78]. [x] Reference [79]. [y] Reference [80]. [z] Reference [81].

All geometric structures for the ground states of H_2, NH_2, NH_3, NH_4, OH, H_2O, H_3O, and its cations are fully optimized with the Hartree–Fock (HF), second–order Möller–Plesset (MP2), and coupled cluster with both single and double substitution [CCSD(t)] levels using GAUSSIAN 98. The excited states of NH_4 and H_3O are somewhat of a Rydberg nature with a cationic core. Therefore, the geometric structures of these states are expected to be similar to those of the corresponding cations. To examine the appropriateness of the procedure, the potential energy of the ground state surface from AH_a to its dissociation products has been calculated with the SDCI and CCSD(t) methods. Meanwhile, to obtain the metastable state of the Rydberg H_2F radical, the geometric structures are optimized using the basis set cited from the Ref. [58]. But, the optimized structure of H_2F could not obtain.

3 RESULTS AND DISCUSSION

3.1 Potential Curves of NH_4 Dissociating into its Asymptotes

The bond lengths at the equilibrium and transition states and the relative energies of the NH_4 radical dissociating into (NH_3 + H) and (NH_2 + H_2) are listed in Table 1 together with the ionization and excitation energies of NH_4, NH_3, and NH_2. Our results for the ammonia molecules [NH_n (n =

2–4)] calculated by SDCI and CCSD(t) are in reasonable agreement with the experimental [1–19,70,75] and theoretical [20–32,71–74,76–81] values. Since the ground state of NH_4 has an electron in a Rydberg 3s orbital, NH_4 itself is often called the Rydberg radical and NH_4 is a semi–ionic state. At the equilibrium geometry of NH_4, $R_{(NH)eq} \cong 1.04$ Å is slightly larger than those [$R_{(NH)eq} \cong 1.01$ Å] of NH_3. For NH_4 dissociating into (NH_3 + H), the bond lengths [$R_{(NH)TS}$] at the transition state is ≅ 1.439 Å. The energy barrier heights of $^2A_1$ from the transition state to NH_4 and (NH_3 + H) are ≅ 0.83 and 0.61 eV, respectively. The energy gap between NH_4 and (NH_3 + H) is –0.22 eV. For NH_4 dissociating into (NH_2 + H_2), the bond lengths [$R_{(NH)TS}$] at the transition state is ≅ 1.590 Å. The energy barrier heights of $^2A_1$ from the transition state to NH_4 and [$NH_2^*(A^2A_1)$ + H_2] are ≅ 3.59 and 1.06 eV, respectively. The heights of $^2B_1$ from the transition state to NH_4 and [$NH_2(X^2B_1)$ + H_2] are ≅ 2.96 and 4.66 eV, respectively. The energy gaps of $^2A_1$ and $^2B_1$ between NH_4 and (NH_2 + H_2) are –2.53 and –1.69 eV, respectively. Although the ground state of the NH_4 radical has an energy barrier of ≅0.83 eV along the NH bond rupture, the stability of NH_4 is influenced by tunneling. The bond breaking takes place near the equilibrium geometry of NH_4. But, the existence of NH_4 has been confirmed by the various methods [20–32]. The lifetime of NH_4 was measured experimentally to be 13 ps, a value more than 10^6 times shorter than in the one for NH_4 in ammonia clusters [1–19].

Smith *et al*. [23,27], Kassab *et al*. [21,22], and Cardy *et al*. [25] have calculated the ground potential energy curve of the NH_4 radical dissociating into (NH_3 + H) and (NH_2 + H_2). Its bond distances at the equilibrium [$R_{(NH)eq}$] obtained by CIPSI (equivalent to a multireference Möller–Plesset second order method) and SDCI are ≅ 1.04 and 1.03 Å, respectively. And the bond distances [$R_{(NH)TS}$] at the transition state are ≅ 1.37 and 1.43 Å, respectively. The barrier heights from the transition state to NH_4 are ≅ 0.88 and 0.85 eV, respectively. The potential curves for the dissociation of NH_4 into its products are endothermic by –0.23 and –0.21 eV, respectively. And the energy gap between (NH_3 + H) and (NH_2 + H_2) is 0.1 eV.

As shown in Table 1, our result for the formation reaction of NH_4 from (NH_2 + H_2) is slightly endothermic by –0.22. By the weak interaction between the nuclear and a Rydberg electron, the ionization and excitation energies of NH_4 are relatively low, that is, the excitation energies of the Rydberg transitions (3s→higher orbitals) should be lower than $E_{(I.P.)} \cong 4.57$ eV. Our results are similar to the other theoretical results [22,23], but different from those characterized by Herzberg [5], that is, the excitation energies of (3s→3d) and (3p→3d) observed by the experiment are 2.19 and 1.87 eV, respectively. Meanwhile, the geometric structure of NH_4 is similar to that of NH_4^+ and the Rydberg NH_4 radical is a semi–ionic structure described as $(NH_4^+)(e^-)_{3s}$. The geometric

structure of NH_4^+ with the T_d symmetry is more stable than that of NH_3 with C_{3v}. Therefore, the proton affinity of NH_3 is relatively large. Since the ionization from NH_3 to NH_3^+ comes to change the geometric structure from the C_{3v} symmetry to D_{3h}, the ionization and excitation energies of NH_2 and NH_3 are relatively large. Our results are in good agreement with the experimental [4,5,11,70,75] and theoretical [22,23,27,30,71–74,76–81] results.

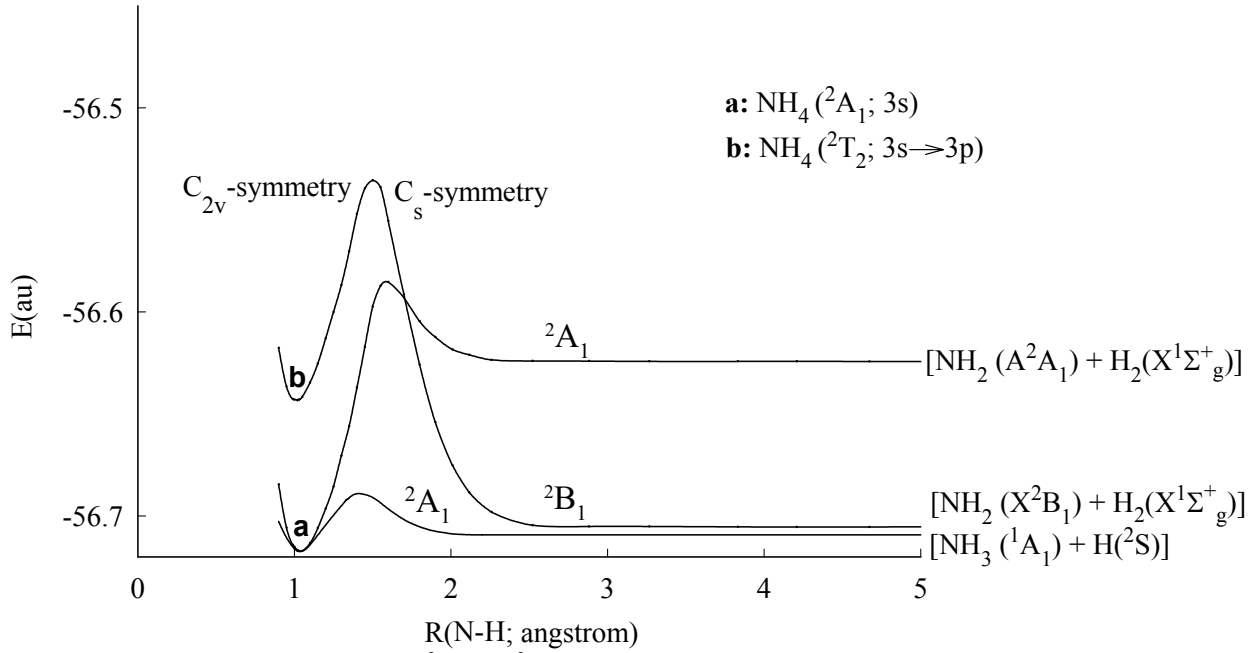

Figure 1. Potential energy curves for the $^2A_1$ and $^2B_1$ states of the Rydberg NH_4 radical dissociating into (NH_3 + H) and (NH_2 + H_2) obtained with the SDCI level.

Under the C_{3v}–, C_{2v}–, and C_s–symmetry constraints, the potential energy curves for the $^2A_1$ and $^2B_1$ states of the Rydberg NH_4 radical dissociating into (NH_3 + H) and (NH_2 + H_2) are drawn in Figure 1. The potential energy curve for the ground state of NH_4 dissociating into (NH_3 + H) is progressed with C_{3v}–symmetry. From equilibrium to $R_{(NH)}$≅2.0 Å, the dissociation reaction of NH_4 into (NH_2 + H_2) is progressed with C_{2v}–symmetry. The potential energy curve of the ground state ($^2A_1$) of NH_4 correlates to the [$NH_2^*(A^2A_1 + H_2(X^1\Sigma_g^+)$) asymptote. From $R_{(NH)}$ ≅ 2.0 Å to their dissociation products, the reaction is progressed with C_s–symmetry. The potential curve correlates to the product limits of [$NH_2(X^2B_1) + H_2(X^1\Sigma_g^+)$]. As the results, the symmetry breaking in the correlation diagram is occurred at $R_{(NH)}$ ≅ 2.0 Å. Cardy *et al*. [25] have analyzed the correlation curves for the dissociation of NH_4 into (NH_2 + H_2) under the C_{2v}– and C_s–symmetry constraints. Their potential curves emerging from the [$NH_2^*(A^2A_1) + H_2(X^1\Sigma_g^+)$] and [$NH_2(X^2B_1) + H_2(X^1\Sigma_g^+)$] asymptotes are crossed behind the rate determining step of the insertion of H_2 into NH_2. The rate determining step of the reaction is not a transition state but a critical point. They have concluded that the insertion process occurs via a two–step mechanism along the crossing of the C_s saddle point.

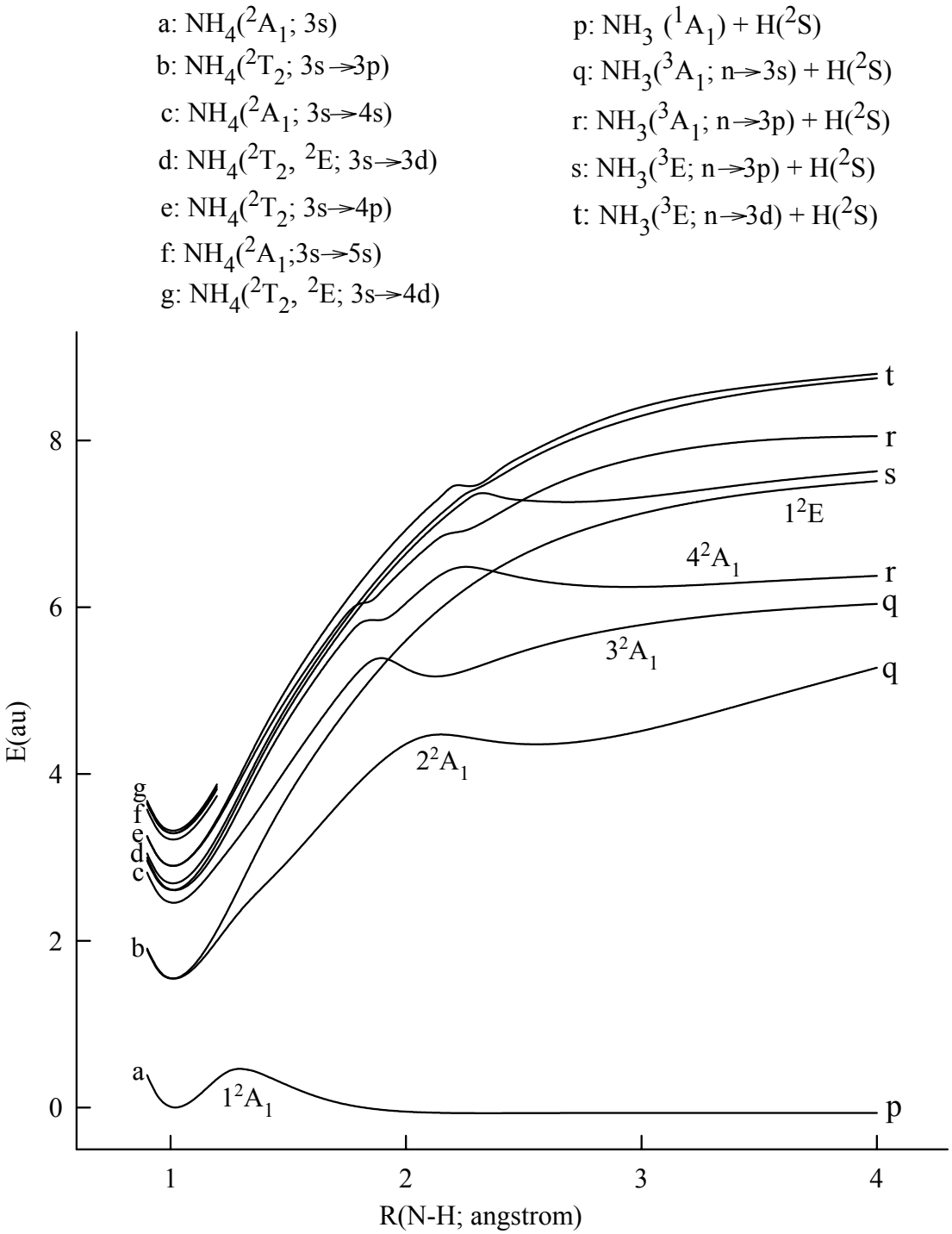

Figure 2. Adiabatic potential energy curves for the ground and excited states of the Rydberg NH_4 radical dissociating into (NH_3 + H).

The potential energy curves for the ground and low lying excited states of the Rydberg NH_4 radical dissociating into (NH_3 + H) are drawn in Figure 2. The potential energy of the NH_4 radical is set equal to zero. Because of the complexity of the excited states, we have cut the potential energy curves of the high lying excited states at $R_{(NH)}$ = 1.2 Å and have not connected the curves between $R_{(NH)}$ = 4.0 Å and the (NH_3 + H) asymptote. We have drawn a few low lying states and they are

labeled as 1^2A_1, 2^2A_1, 3^2A_1, 4^2A_1, and 1^2E. The ground $^2A_1$ state of the NH_4 radical correlates with an antibonding interaction of the [$NH_3(^1A_1)$ + $H(^2S)$] asymptote. This curve is quasibound, which means that its equilibrium energy is higher than that of the dissociation asymptote of (NH_3 + H). The potential curve has a potential barrier near the equilibrium geometry of NH_4. It is made by an avoided curve crossing between the dissociative diabatic state of the Rydberg [$(NH_4^+)(e^-)_{3s}$] radical and the repulsive diabatic state emerging from an antibonding interaction of the [$NH_3(^1A_1)$ + $H(^2S)$] asymptote. The barrier height and potential well are very low and shallow, respectively. The maximum position [$R_{(NH)} \cong 1.40$ Å] of the transition state of the ground potential curve is located out of line of those [$R_{(NH)} \cong 1.95$ Å] of the first and second excited states with the $^2A_1$ symmetry.

In Figure 2, all potential curves of the excited states are shallowly bound. While, the third excited $^2A_1$ state is bound at relatively wide range (between $R_{(NH)} \cong 2.0$ and 6.0 Å). All potential barriers of the excited states are formed by the curve crossings. The first curve crossings between the dissociative diabatic excited states of [$(NH_4^+)(e^-)_{Rydberg}$] and the repulsive diabatic states from the antibonding interaction of [$NH_3(^1A_1)$ + $H(^2S)$] are found between $R_{(NH)} \cong 1.6$ and 2.0 Å. The second curve crossings between the dissociative diabatic excited states of [$(NH_4^+)(e^-)_{Rydberg}$] and the repulsive diabatic states from the antibonding interaction of [$NH_3(^3A_1; n\rightarrow 3s)$ + $H(^2S)$] are also found from $R_{(NH)} \cong 2.0$ to 2.25 Å. The first excited ^2E state emerging from NH_4 ($3s\rightarrow 3p_{x,y}$) directly correlates with an attractive state from the [$NH_3^+(e^-)_{3px,y}$ + H] asymptote. The second excited ^2E state is bound at wide range [between $R_{(NH)} \cong 2.5$ and 6.0 Å]. The wide potential well is made from curve crossing between the dissociative diabatic excited state of [$(NH_4^+)(e^-)_{Rydberg}$] and the repulsive diabatic state emerging from an antibonding interaction of [$NH_3(^3E)$ + $H(^2S)$]. The potential barrier by the avoided curve crossing exists at $R_{(NH)} \cong 2.2$ Å.

Adiabatic and diabatic potential energy curves of the dissociation of NH_4 into (NH_3 + H) have been constructed by Kassab and Evleth [21,22]. According to their curves, the ground $^2A_1$ state surface along the NH bond rupture has a potential energy barrier which is made from the avoided curve crossing. In the diabatic potential curves, the diabatic curve crossings between the repulsive state emerging from (NH_3 + H) and the dissociative states of the ground and excited $^2A_1$ states of NH_4 have been drawn by the broken lines. But, in the adiabatic curves, the potential wells and barriers formed by the avoided crossings have not been represented clearly. And the maximum positions of the potential barriers for the ground and excited potential curves are drawn to be out of line of the repulsive diabatic curve emerging from the (NH_3 + H) asymptote. Particularly, in their Figure 2, the adiabatic and diabatic potential correlation curves with the $^2A_1$ symmetry are quite different from each other.

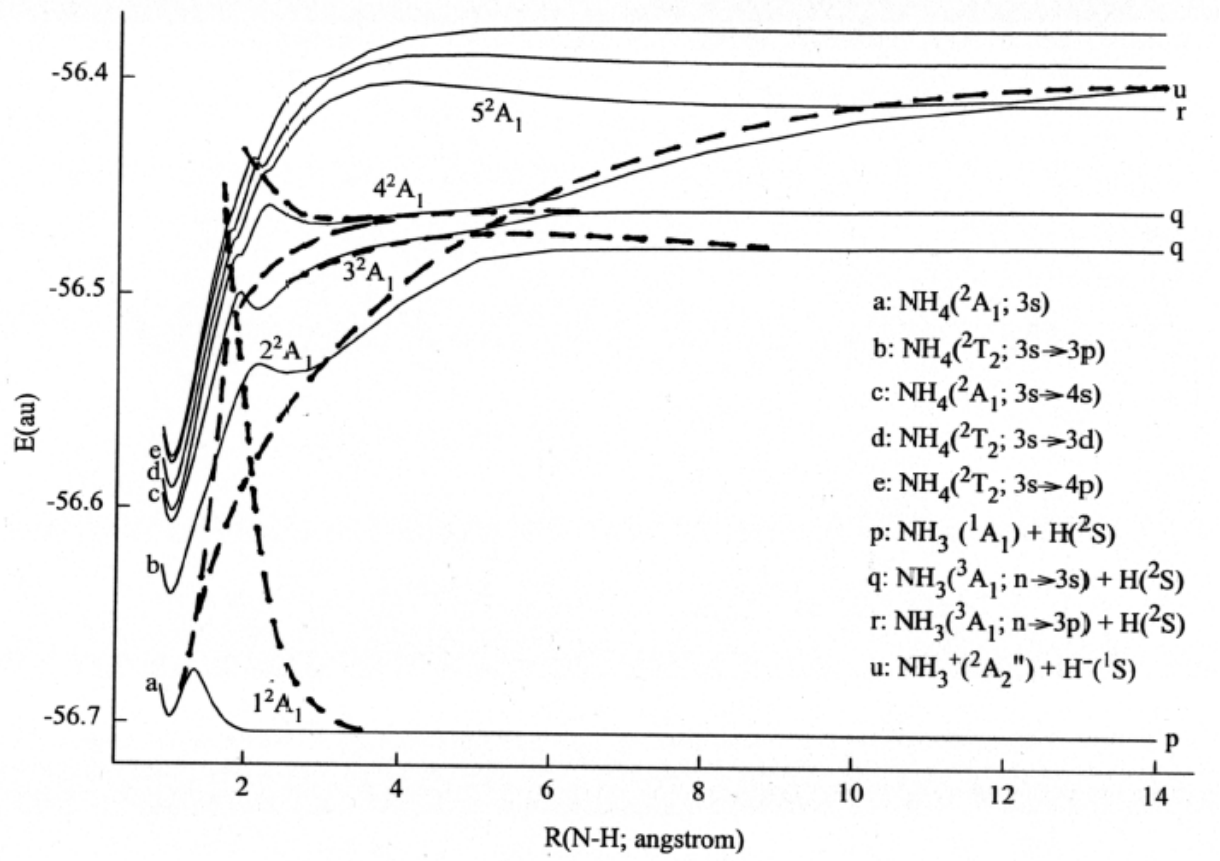

Figure 3. Avoided curve crossings for the $^2A_1$ states of the Rydberg NH_4 radical dissociating into (NH_3 + H). Broken lines indicate estimated diabatic potential curves.

To investigate the avoided curve crossing clearly, the potential energy curves for the ground and low lying excited $^2A_1$ states are presented in Figure 3. The broken lines indicate estimated diabatic potential energy curves and these are drawn by hands. The ground $^2A_1$ state interconnects the NH_4 structure with the (NH_3 + H) asymptote. In the NH_4 radical dissociating into (NH_3 + H), the ground Rydberg NH_4 radical diabatically dissociates into two kinds of the asymptotes, that is, NH_4 diabatically dissociates into the first excited $[(H_3N^+)(e^-)_{3s} + H(^2S)]$ and the ion–ion pair $[H_3N^+(^2A_2'') + H^-(^1S)]$ asymptotes. In the second dissociation, the pair has strongly attractive ion character as an ion approaches to the other. The diabatic potential well should be very deep. As the result, the avoided curve crossings take place around $R_{(NH)} \cong 1.5$ Å. The barrier height of the ground correlation curve is found to be low.

As shown in Figure 3, the 2^2A_1 state is shallowly bound. The barrier around $R_{(NH)} \cong 2.0$ Å is formed from the curve crossing between the attractive state from $[NH_3^+ + H^-]$ and the repulsive state from [NH_3 + H]. The 3^2A_1 state emerging from the $[(NH_3^+)(e^-)_{3s} + H(^2S)]$ asymptote is diabatically repulsive. By the avoided curve crossings, this state is very shallowly bound around $R_{(NH)} \cong 2.0$ Å. The 4^2A_1 state is widely bound due to two avoided curve crossings between $R_{(NH)} \cong 2.0$ and 6.0 Å. Meanwhile, when the internuclear distance between NH_3^+ and H^- become short, the attractive state emerging from an ion–ion pair $[NH_3^+ + H^-]$ diabatically correlates with

NH_4. This state is diabatically bound due to the strongly ion–ion electrostatic attraction. Therefore, around three positions ($R_{(NH)} \cong$ 2.0, 6.0, and 12.0 Å), the curve crosses with the diabatic potential curves of the $^2A_1$ states emerging from the different asymptotes.

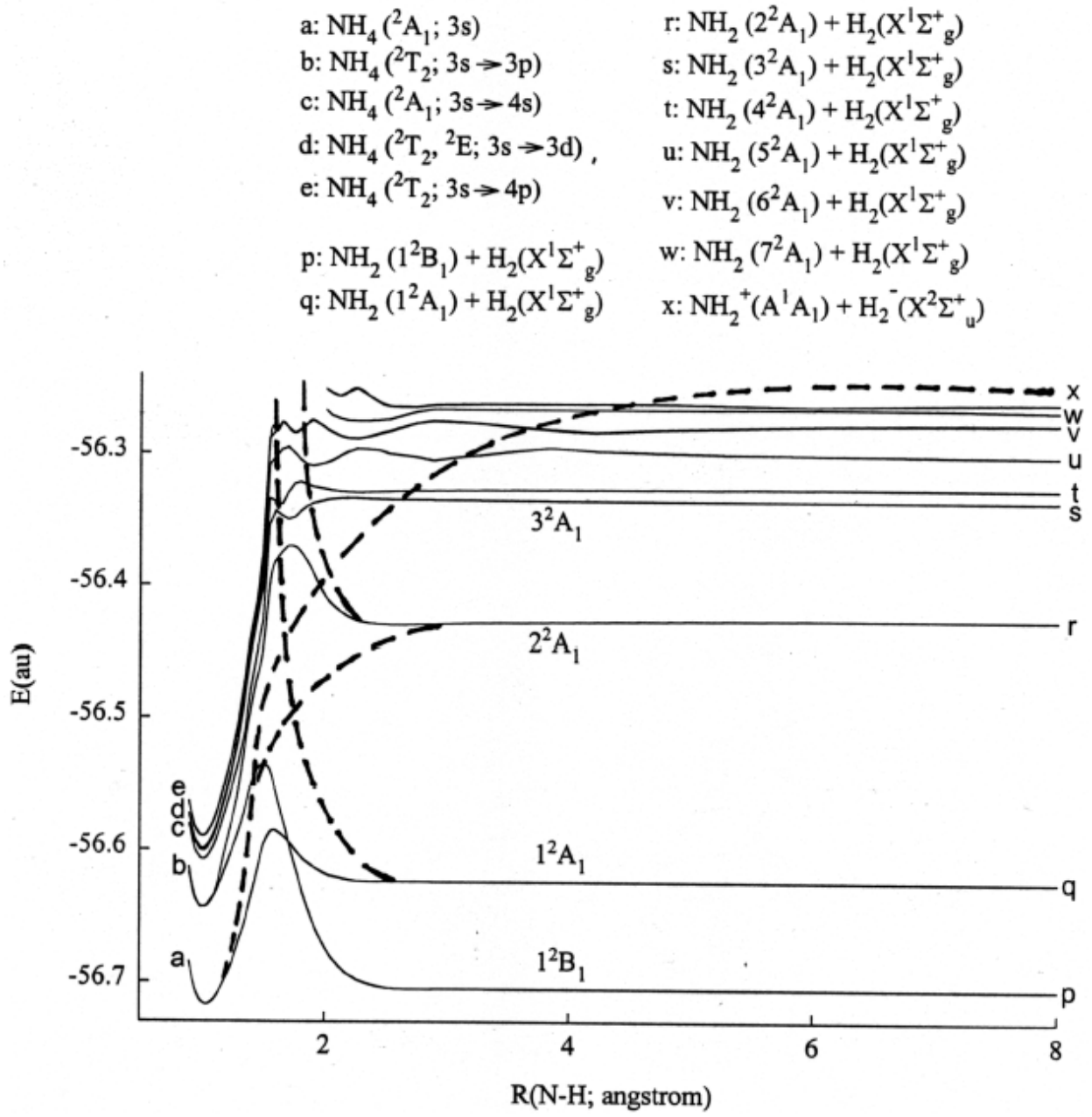

Figure 4. Avoided curve crossings for the $^2A_1$ states of the Rydberg NH_4 radical dissociating into (NH_2 + H_2). Broken lines indicate estimated diabatic potential curves.

The potential energy curves for the several low lying $^2A_1$ states of the Rydberg NH_4 radical dissociating into (NH_2 + H_2) are drawn in Figure 4. And they are labeled as 1^2A_1, 2^2A_1, 3^2A_1, and 1^2B_1. The ground $^2A_1$ state of the NH_4 radical correlates to the [$NH_2^*(1^2A_1)$ + $H_2(X^1\Sigma_g^+)$] asymptote. The potential curve has a potential barrier near the equilibrium geometry of NH_4. It is made by an avoided curve crossing between the dissociative diabatic state of the Rydberg

$[(NH_4^+)(e^-)_{3s}]$ radical and the repulsive diabatic state emerging from an antibonding interaction of the $[NH_2^*(1^2A_1) + H_2(X^1\Sigma_g^+)]$ asymptote. The barrier height and potential well are slightly high and shallowly bound, respectively. The energy gap between $[NH_2(1^2B_1) + H_2(X^1\Sigma_g^+)]$ and $[NH_2^*(1^2A_1) + H_2(X^1\Sigma_g^+)]$ is 2.21 eV.

Table 2. Contributions of the dominant configuration for the low lying Rydberg $^2A_1$ states along the NH_4 radical dissociating into (NH_3 + H). 222210 denotes $2a_1^2\ 1t_1^6\ 3a_1^1\ 4a_1^0$ configuration

$R_{(NH)}$(Å)	1^2A_1		2^2A_1		3^2A_1		4^2A_1	
0.9	22221	0.9983	22220001	0.9989	222200001	0.9997	222200000001	0.9998
1.0	22221	0.9982	22220001	0.9986	222200001	0.9997	222200000001	0.9997
1.1	22221	0.9977	22220100	0.9978	222200001	0.9993	222200000100	0.9992
1.2	22221	0.9962	22220100	0.9954	222200001	0.9972	222200000100	0.9984
1.4	22221	0.9857	22220100	0.9827	222200001	0.9914	222200000100	0.9959
1.5	22221	0.9801	22220100	0.9771	222200001	0.9986	222200000100	0.9901
			22211100	0.0319				
			22212000	0.0861				
1.6	22221	0.9760	22220100	0.9681	222200001	0.9837	222200000100	0.9794
			22211100	0.0820				
			22212000	0.1056				
1.8	22221	0.9692	22220100	0.9322	222200001	0.9261	222200000100	0.8419
			22211100	0.1475				
			22212000	0.1740				
2.0	22221	0.9631	22220100	0.8301	222120000	0.7155	222200001000	0.8618
			22211100	0.2357				
			22212000	0.3679				
2.1	22221	0.9600	22220100	0.6953	222120000	0.6190	222200001000	0.8343
			22211100	0.2807				
			22212000	0.5426				
2.2	22221	0.9568	22212000	0.6818	222201000	0.6599	222200001000	0.6794
			22211100	0.3015				
2.3	22221	0.9537	22212000	0.7450	222201000	0.7056	222111000000	0.6523
			22211100	0.3064				
2.5	22221	0.9480	22212000	0.7775	222201000	0.6856	222111000000	0.6997
			22211100	0.3139				
3.0	22221	0.9391	22212000	0.7646	222201000	0.5295	222111000000	0.6870
			22211100	0.3537				
3.5	22221	0.9379	22212000	0.7375	222201000	0.3814	222111000000	0.6525
			22211100	0.4031				
4.0	22221	0.9397	22212000	0.7009	222120000	0.4036	222110100000	0.5200
	22221		22211100	0.4500				
5.0	22221	0.9425	22211100	0.4915	222120000	0.5805	222110100000	0.6064
6.0	22221	0.9437	22211010	0.5458	222110100	0.6164	222120000000	0.7491
7.0	22221	0.9444	22211010	0.5709	222110100	0.6865	222120000000	0.7970
8.0	22221	0.9450	22211010	0.5720	222110100	0.6923	222120000000	0.8065
10.0	22221	0.9462	22211010	0.5517	222110100	0.6715	222120000000	0.8168
12.0	22221	0.9468	22211010	0.5298	222110100	0.6474	222110100000	0.6138
14.0	22221	0.9473	22211010	0.5151	222110100	0.6299	222110100000	0.6522

All potential energy curves emerging from the antibonding interactions of the $[NH_2^*(^2A_1) + H_2(X^1\Sigma_g^+)]$ asymptotes are diabatically repulsive, while a potential energy curve emerging from the $[NH_2^+(A^1A_1) + H_2^-(X^2\Sigma_u^+)]$ asymptote is diabatically attractive. As a results, at shorter than $R_{(NH)} \cong 2.0$ Å, the avoided curve crossings between the dissociative diabatic states of $[(NH_4^+)(e^-)_{Rydberg}]$ and the repulsive diabatic states from $[NH_2 + H_2(X^1\Sigma_g^+)]$ are occurred. At larger

than $R_{(NH)} \cong 2.0$ Å, the curve crossings between the diabatically attractive diabatic state emerging from [$NH_2^+(A^1A_1)$ + $H_2^-(X^2\Sigma_u^+)$] and the diabatically repulsive diabatic states from [NH_2 + $H_2(X^1\Sigma_g^+)$] are found. Therefore, all potential barriers of the $^2A_1$ states are formed by the curve crossings.

Table 3. Contributions of the dominant configuration for the low lying Rydberg $^2A_1$ states along the NH_4 radical dissociating into (NH_2 + H_2). 222210 denotes $2a_1^2\ 1t_1^6\ 3a_1^1\ 4a_1^0$ configuration

$R_{(NH)}$(Å)	1^2A_1		2^2A_1		3^2A_1	
0.9	222210	0.9987	22220001	0.9989	222200001	0.9897
1.0	222210	0.9981	22220001	0.9982	222200001	0.9853
1.1	222210	0.9976	22220001	0.9878	222200001	0.9834
1.2	222210	0.9960	22120200	0.9954	221202000	0.6798
1.4	222210	0.9872	22120200	0.9827	221202000	0.6972
1.5	222210	0.9753	22202100	0.5978	222012000	0.5596
			22201200	0.0861		
1.6	222102	0.9892	22202100	0.5788	222012000	0.5982
			22201200	0.1056		
1.8	222102	0.9914	22202100	0.5523	222002100	0.6056
			22201200	0.2475		
2.0	221202	0.8848	22202100	0.5311	222002100	0.6937
			22201200	0.4357		
2.1	221202	0.9105	22201200	0.6653	222002100	0.7298
2.2	221202	0.9289	22201200	0.6818	222002100	0.7677
2.3	221202	0.9493	22201200	0.7450	222002100	0.7993
2.5	221202	0.9546	22201200	0.7775	222012000	0.8579
3.0	221202	0.9633	22201200	0.8273	222012000	0.8992
3.5	221202	0.9686	22201200	0.8976	222012000	0.9215
4.0	221202	0.9720	22201200	0.9380	222012000	0.9249
5.0	221202	0.9731	22201200	0.9542	222012000	0.9308
6.0	221202	0.9739	22201200	0.9583	222012000	0.9394
7.0	221202	0.9746	22201200	0.9606	222012000	0.9417
8.0	221202	0.9751	22201200	0.9706	222012000	0.9426

Adiabatic potential energy curves for the dissociation of NH_4 into (NH_2 + H_2) have been constructed by Kassab and Evleth [21,22] and Cardy *et al*. [25]. In the potential energy curve of Kassab and Evleth, the three states emerging from the dissociative states of NH_4 directly correlates to the three repulsive states from the (NH_2 + H_2) asymptote under the C_{2v}–symmetry constraints. By the avoided curve crossings between the dissociative states and the repulsive states, the barriers are formed at shorter than $R_{(NH)} \cong 2.0$ Å. When H_2 molecule approaches the three valence states of NH_2, these states are repulsive. Particularly, Cardy *et al*. has analyzed the detailed geometric representation of the insertion mechanism, the quantitative state correlation diagram, and the relaxation of a C_{2v} reaction path between NH_4 and (NH_2 + H_2). The quantitative state correlation diagram and relaxation of a C_{2v} reaction path have been represented in detail. But the adiabatic potential curves and barriers formed by the avoided crossings have not been represented clearly.

Now the question is why the maximum positions of the ground and excited states are found to be out of line of the repulsive diabatic curve emerging from the antibonding interaction of [$NH_3(^1A_1)$ + $H(^2S)$] and [NH_2 + $H_2(X^1\Sigma_g^+)$]. To analyze the curve crossing, we have investigated the

contributions of the dominant configuration to the total wave functions of the $^2A_1$ states and listed them in Table 2 and 3. For NH_4 dissociating into (NH_3 + H) and (NH_2 + H_2), the dominant configuration for the ground $^2A_1$ state is [core]$2a_1^2$ $1t_1^6$ $3a_1^1$ at the NH_4 structure, [core]$2a_1^2$ $1e_1^4$ $3a_1^2$ $(4a_1^1)_H$ at the (NH_3 + H) asymptote, and [core]$2a_1^2$ $1b_2^2$ $3a_1^1$ $1b_1^2$ $(5a_1^2)_{H2}$ at the (NH_2 + H_2) asymptote. $2a_1^2$ $1t_1^6$ is an electronic configuration of NH_4^+. $3a_1^1$ indicates an electron of the Rydberg 3s orbital having a NH_4^+ structure as a core. Therefore, the electronic structure of NH_4 indicates as $NH_4^+(e^-)_{3s}$. Along N–H bond rupture, a $1t_1$ orbital of NH_4 separates into two orbitals ($1e_1$ and $3a_1$) in NH_3. The $4a_1$ orbital is nonbonding, *i.e.*, a character of 1s of H. $4a_1^1$ indicates one electron in the 1s orbital of H. As the result, the configuration of $2a_1^2$ $1e_1^4$ $3a_1^2$ $(4a_1^1)_H$ at $R_{(NH)}$ = 14.0 Å indicates the antibonding pair [$NH_3(^1A_1)$ + $H(^2S)$] asymptote. For NH_2–H_2 bond rupture, a $1t_1$ orbital of NH_4 separates into two orbitals ($1b_2$ and $3a_1$) in NH_2. The $5a_1$ orbital is a character of 1σ of H_2. $5a_1^2$ indicates two electrons in the 1σ orbital of H_2. Therefore, the configuration of $2a_1^2$ $1b_2^2$ $3a_1^1$ $1b_1^2$ $(5a_1^2)_{H2}$ at $R_{(NH)}$ = 8.0 Å indicates the antibonding pair [$NH_2^*(1^2A_1)$ + $H_2(X^1\Sigma_g^+)$] asymptote.

As shown in Table 2, the dominant configurations of the [$H_3N(^3A_1;n\rightarrow3s)$ + $H(^2S)$] and [$NH_3^+(^2A_2'')$ + $H^-(^1S)$] asymptotes are <u>222111</u> and <u>22212</u>, respectively. In the diabatic dissociation of NH_4 into [$(H_3N^+)(e^-)_{3s}$ + $H(^2S)$], the contribution for the configuration of <u>222111</u> begins to appear the first excited $^2A_1$ state at $R_{(NH)}$ = 1.5 Å and the contribution of it increases with internuclear distance. From $R_{(NH)}$ = 5.0 Å, it become a dominant configuration in the first $^2A_1$ state. In the diabatic dissociation of NH_4 into the ion–ion pair [$H_3N^+(^2A_2'')$ + $H^-(^1S)$] asymptote, the contribution for the configuration of <u>22212</u> represents the first excited $^2A_1$ state from $R_{(NH)}$ = 1.5 to 4.0 Å. At $R_{(NH)}$ = 5.0 Å, the contribution represents the second excited state. Between $R_{(NH)}$ = 6.0 and 10.0 Å, it represents the third excited state. This configuration can have an attractive ion character as an ion approaches another. These two attractive diabatic curves cross with the repulsive diabatic curve emerging from an antibonding interaction of the [$NH_3(^1A_1)$ + $H(^2S)$] asymptote. Two attractive diabatic characters greatly influence the curve crossing, that is, the contributions of those characters are larger than that of the repulsive character. As the result, the potential energy barrier of the ground $^2A_1$ state is shifted to the equilibrium geometry of NH_4. And the barrier height appears to be low. Particularly, the avoided curve crossing between repulsive curve emerging from an antibonding interaction of the [$NH_3(^1A_1)$ + $H(^2S)$] and the strongly attractive curve from [$H_3N^+(^2A_2'')$ + $H^-(^1S)$] greatly influences the potential barrier of the ground correlation curve.

In the excited 2^2A_1 state, the dominant configuration is $2a_1^2$ $1t_1^6$ $(3p_z)^1_{Rydberg}$ at shorter than $R_{(NH)} \cong$ 1.1 Å, $2a_1^2$ $1e_1^4$ $3a_1^2$ $(3p_z)^1_{Rydberg}$ between $R_{(NH)} \cong$1.1 and 2.1 Å, $(2a_1')^2$ $(1e_1')^4$ $(1a_2'')^1$ $(1s)^2_H$ between $R_{(NH)} \cong$ 2.2 and 4.0 Å, and $(2a_1')^2$ $(1e_1')^4$ $(1a_2'')^1$ $(3s)^1_{Rydberg}$ $(1s)^1_H$ at larger than $R_{(NH)} \cong$ 5.0 Å. In the dissociation of NH_4 into (NH_3 + H), $2a_1^2$ $1t_1^6$ $(3p_z)^1_{Rydberg}$ at shorter than $R_{(NH)} \cong$ 1.1 Å represents the $(NH_4^+)(e^-)_{3pz}$ structure, $2a_1^2$ $1e_1^4$ $3a_1^2$ $(3p_z)^1_{Rydberg}$ between $R_{(NH)} \cong$ 1.1 and 2.1 Å represents $(NH_3\ldots H^+)(e^-)_{3pz}$, $(2a_1')^2$ $(1e_1')^4$ $(1a_2'')^1$ $(1s)^2_H$ between $R_{(NH)} \cong$ 2.2 and 4.0 Å represents

$(NH_3^+ \ldots H^-)$, and $(2a_1')^2\ (1e_1')^4\ (1a_2'')^1\ (3s)^1_{Rydberg}\ (1s)^1_H$ at larger than $R_{(NH)} \cong 5.0$ Å represents $[(H_3N^+)(e^-)_{3s} + H]$. More interestingly, the 2^2A_1 state between $R_{(NH)} \cong 2.2$ and 4.0 Å has a dominant configuration of $(2a_1')^2\ (1e_1')^4\ (1a_2'')^1\ (1s)^2_H$ which means an ion–ion interaction structure as $(NH_3^+ \ldots H^-)$. Here one electron jumped from the Rydberg $3p_z$ orbital of NH_3 to the 1s orbital of H. Therefore, this state has strongly attractive ion character.

The dominant configuration of the 3^2A_1 state is $2a_1^2\ 1t_1^6\ (4s)^1_{Rydberg}$ at shorter than $R_{(NH)} \cong 2.0$ Å, $(2a_1')^2\ (1e_1')^4\ (1a_2'')^1\ (1s)^2_H$ between $R_{(NH)} \cong 2.0$ and 2.1 Å, $2a_1^2\ 1e_1^4\ 3a_1^2\ (3p_z)^1_{Rydberg}$ between $R_{(NH)} \cong 2.2$ and 3.5 Å, $(2a_1')^2\ (1e_1')^4\ (1a_2'')^1\ (1s)^2_H$ between $R_{(NH)} \cong 4.0$ and 5.0 Å, and $(2a_1')^2\ (1e_1')^4\ (1a_2'')^1\ (3s)^1_{Rydberg}\ (1s)^1_H$ at larger than $R_{(NH)} \cong 5.0$ Å. In the electronic structure, $2a_1^2\ 1t_1^6\ (4s)^1_{Rydberg}$ represents $(NH_4^+)(e^-)_{4s}$, $(2a_1')^2\ (1e_1')^4\ (1a_2'')^1\ (1s)^2_H$ represents $(NH_3^+ \ldots H^-)$, $2a_1^2\ 1e_1^4\ 3a_1^2\ (3p_z)^1_{Rydberg}$ represents $[(NH_3)\ldots(H^+)](e^-)_{3pz}$, and $(2a_1')^2\ (1e_1')^4\ (1a_2'')^1\ (3s)^1_{Rydberg}\ (1s)^1_H$ represents $[(NH_3^+)(e^-)_{3s} + H]$. Around $R_{(NH)} \cong 2.05$ and 4.5 Å, the dominant configuration represents $(2a_1')^2\ (1e_1')^4\ (1a_2'')^1\ (1s)^2_H$ which means the attractive interaction of $[NH_3^+ \ldots H^-]$. In the 4^2A_1 state, the dominant configuration between $R_{(NH)} \cong 2.3$ and 5.0 Å is $(2a_1')^2\ (1e_1')^4\ (1a_2'')^1\ (3s)^1_{Rydberg}\ (1s)^1_H$ of a repulsive character emerging from the $[(NH_3^+)(e^-)_{3s} + H]$ asymptote. The dominant configuration between $R_{(NH)} \cong 6.0$ and 10.0 Å is $(2a_1')^2\ (1e_1')^4\ (1a_2'')^1\ (1s)^2_H$ having the $(NH_3^+ + H^-)$ character. The changes of these configurations are in accordance with the potential energy curves in Figure 3.

As shown in Table 3, the dominant configurations of the $[H_2N(2^2A_1;n\rightarrow 3s) + H_2(X^1\Sigma_g^+)]$ and $[NH_2^+(A^1A_1) + H_2^-(X^2\Sigma_u^+)]$ asymptotes are <u>222012</u> as a $[\text{core}]2a_1^2\ 1b_2^2\ 3a_1^2\ 1b_1^0\ 4a_1^1\ (5a_1^2)_{H2}$ configuration and <u>222021</u> as a $[\text{core}]2a_1^2\ 1b_2^2\ 3a_1^2\ 1b_1^0\ (5a_1^2\ 6a_1^1)_{H2}$, respectively. In the diabatic dissociation of NH_4 into $[(H_2N)(e^-)_{3s} + H_2(X^1\Sigma_g^+)]$, the contribution for the configuration of <u>222012</u> begins to appear in 2^2A_1 at $R_{(NH)} = 1.5$ Å and the contribution of it increases with internuclear distance. From $R_{(NH)} = 2.1$ Å, it become a dominant configuration in 2^2A_1. In the diabatic dissociation of NH_4 into the ion–ion pair $[NH_2^+(A^1A_1) + H_2^-(X^2\Sigma_u^+)]$ asymptote, the contribution for the configuration of <u>222021</u> is represented in the 2^2A_1 state from $R_{(NH)} = 1.5$ to 2.0 Å. Although the configurations from 4^2A_1 to 7^2A_1 have not listed in Table 3, the contribution will be represented between $R_{(NH)} = 2.2$ and 8.0 Å. The attractive diabatic character greatly influences the curve crossing. As a result, the potential energy barriers of the 1^2A_1 and 2^2A_1 states are shifted to the equilibrium geometry of NH_4.

In the excited 2^2A_1 state, the dominant configuration is $2a_1^2\ 1t_1^6\ (3p_z^1)_{Rydberg}$ at shorter than $R_{(NH)} \cong 1.1$ Å, $2a_1^2\ 1b_2^2\ 3a_1^1\ 1b_1^2\ (5a_1^2)_{Rydberg}$ between $R_{(NH)} \cong 1.2$ and 1.4 Å, $2a_1^2\ 1b_2^2\ 3a_1^2\ 1b_1^0\ (5a_1^2\ 6\ a_1^1)_{H2}$ between $R_{(NH)} \cong 1.5$ and 2.0 Å, and $2a_1^2\ 1b_2^2\ 3a_1^2\ 1b_1^0\ (4a_1^1)_{Rydberg}\ (5a_1^2)_{H2}$ at larger than $R_{(NH)} \cong 2.1$ Å. In the electron structure, $2a_1^2\ 1t_1^6\ (3p_z^1)_{Rydberg}$ at shorter than $R_{(NH)} \cong 1.1$ Å represents the $(NH_4^+)(e^-)_{3pz}$ structure, $2a_1^2\ 1b_2^2\ 3a_1^1\ 1b_1^2\ (5a_1^2)_{Rydberg}$ between $R_{(NH)} \cong 1.2$ and 1.4 Å represents $(NH_2\ldots H_2)^+(e^-)_{3pz}$, $2a_1^2\ 1b_2^2\ 3a_1^2\ 1b_1^0\ (5a_1^2\ 6a_1^1)_{H2}$ between $R_{(NH)} \cong 1.5$ and 2.0 Å represents $(NH_2^+ \ldots H_2^-)$, and $2a_1^2\ 1b_2^2\ 3a_1^2\ 1b_1^0\ (4a_1^1)_{Rydberg}\ (5a_1^2)_{H2}$ at larger than $R_{(NH)} \cong 2.1$ Å

represents $[(H_2N^+)(e^-)_{3s} + H_2]$. Particularly, the dominant configuration of 2^2A_1 between $R_{(NH)} \cong 1.5$ and 2.0 Å means an ion–ion interaction structure $(NH_2^+ \ldots H_2^-)$ as $2a_1^2\ 1b_2^2\ 3a_1^2\ [(1\sigma)^2\ (1\sigma^*)^1]_{H2}$.

Table 4. Bond lengths (Å), angle (degree), and relative energies (eV) for the H_3O radical dissociating into (H_2O + H) and (OH + H_2). Ionization and excitation energies (eV) of H_3O, H_2O, OH, and H_2

	HF	SECI[a]	SDCI[a]	MP2[b]	CCSD(t)[b]	HF[c]	CI[d]	CEPA[e]	exptl
X^2A_1 state emerging from (H_2O + H)									
$R_{(OH)eq}$	0.984	0.984	1.018	1.021	1.020	0.984	1.053	1.02	
$(\angle HOH)_{eq}$	107.6	106.3	106.0	105.7	105.9	111.8	101.8	106.9	
$R_{(OH)TS}$	1.174	1.122	1.213	1.215	1.210	1.21	1.248		
$\Delta E_{(H3O–TS)}$	0.19	0.13	0.12	0.11	0.11	0.29	0.13	0.08	
$\Delta E_{[TS–(H2O+H)]}$	1.45	1.07	0.97	1.01	0.93	1.51	1.02	1.08	
$\Delta E_{[H3O–(H2O+H)]}$	–1.27	–0.94	–0.86	–0.90	–0.82	–1.22	–0.89	–1.0	
X^2A_1 state emerging from (OH + H_2)									
$R_{(OH)eq}$	1.009	1.026	1.031	1.021	1.020		0.984	1.053	1.02
$R_{(OH)TS}$	1.467	1.510	1.513				1.248		
$\Delta E_{(H3O–TS)}$		5.24	4.99				0.13[f]	0.08[f]	
$\Delta E_{[TS–(OH+H2)]}$		1.27	1.14				1.02[f]	1.08[f]	
$\Delta E_{[H3O–(OH+H2)]}$		–3.97	–3.85				–0.89[f]	–1.0[f]	
A^2B_1 state emerging from (OH + H_2)									
$R_{(OH)eq}$		1.014	1.019						
$R_{(OH)TS}$		1.492	1.501						
$\Delta E_{(H3O–TS)}$		5.11	5.02						
$\Delta E_{[TS–(OH+H2)]}$		7.36	7.18						
$\Delta E_{[H3O–(OH+H2)]}$		–2.24	–2.15						
H_3O									
I.E.[g]	4.73	4.95	5.30	5.32	5.34	5.36	4.68[h]	5.36	4.34[k]
							4.30[i]	4.43[j]	4.4[l]
							4.17[i]		
$\Delta E_{(3s–3p)}$;$^2A_1$,^2E		2.09	1.92				1.87[h]	2.65	1.7[k]
$\Delta E_{(3s–4s)}$;$^2A_1$		2.72	2.80					3.18	
$\Delta E_{(3s–3d)}$;$^2A_1$		2.99	3.04					3.71	
H_2O									
I.E.[g]	11.06	12.50	12.54	12.56	12.52		12.63[n]		12.6[p,q]
P.A.[m]	7.60	7.44	7.32	7.39	7.30		7.45[n]	7.22	7.18[p]
							7.79[o]	7.13	
$\Delta E_{(1b1–3s)}$; A^1B_1		6.90	6.51						6.67[q]
$\Delta E_{(1b1–3px,y)}$; D^1A_1		10.27	10.21						10.17[q]
OH									
I.P.[g]	11.32	12.42	12.71	12.75	12.70	12.38[s]	11.27[t]	11.44[x]	15.759[A]
							13.36[u]	15.53[y]	
E.A.[r]	1.54	1.73	1.81	1.91	1.85	1.48[s]	1.91[v]	5.652[y]	1.83[B]
$\Delta E_{(X2\Pi–A2\Sigma+)}$		3.98	4.11			3.95[s]	4.17[w]	4.0[z]	4.05[C]
$\Delta E_{(X2\Pi–4\Sigma–)}$		7.04	7.33				7.65[w]	6.9[z]	
$\Delta E_{(X2\Pi–2\Sigma–)}$		7.96	8.28				8.51[w]	7.9[z]	
$\Delta E_{(X2\Pi–2\Delta)}$		9.87	10.16				10.37[w]	9.9[z]	
$\Delta E_{(X2\Pi–2\Pi)}$		10.48	10.75					10.6[z]	
$\Delta E_{(X2\Pi–4\Pi)}$		10.49	10.77				11.09[w]	10.6[z]	

Table 4. (Continued)

	HF	SECI[a]	SDCI[a]	MP2[b]	CCSD(t)[b]	HF[c]	CI[d]	CEPA[e]	exptl
$\Delta E_{(X2\Pi-2\Sigma+)}$		11.87	11.52				11.31[w]	11.50[z]	
H_2									
I.P.[g]	14.52	15.21	15.43	15.25	15.46	15.43	14.55[t]		13.36[x]
E.A.[r]	1.26	1.33	1.38	1.35	1.39	1.48			1.38[x]

[a] SECI and SDCI energies were obtained with the MOs and geometries of H_3O^+ calculated by RHF at each internuclear distance. [b] Values were obtained with Gaussian 98. [c] Reference [44]. [d] Reference [46]. [e] Reference [49]. [f] Potential energy gaps between each states on the surface of H_3O dissociating (OH + H_2). [g] Ionization potential energies of H_3O, H_2O, OH, and H_2. [h] Reference [47]. [i] Reference [43]. [j] Reference [37]. [k] Reference [40]. [l] Reference [10]. [m] Electronic energy difference between H_2O and H_3O^+. [n] Reference [82]. [o] Reference [83]. [p] Reference [84]. [q] Reference [85]. [r] Electron affinity of OH and H_2. [s] Reference [86]. [t] Reference [87]. [u] Cited from Reference [88]. [v] Reference [89]. [w] Reference [90]. [x] Reference [88]. [y] Reference [91]. [z] Reference [92]. [A] Reference [93]. [B] Reference [94]. [C] Reference [95].

The dominant configuration of the 3^2A_1 state is $2a_1^2\ 1t_1^6\ (4s^1)_{Rydberg}$ at shorter than $R_{(NH)} \cong 1.1$ Å, $2a_1^2\ 1b_2^2\ 3a_1^1\ 1b_1^2\ (5a_1^2)_{Rydberg}$ between $R_{(NH)} \cong 1.2$ and 1.4 Å, $2a_1^2\ 1b_2^2\ 3a_1^2\ 1b_1^0\ (4a_1^1)_{Rydberg}\ (5a_1^2)_{H2}$ between $R_{(NH)} \cong 1.5$ and 1.6 Å, $2a_1^2\ 1b_2^2\ 3a_1^2\ 1b_1^0\ (5a_1^2\ 6a_1^1)_{H2}$ between $R_{(NH)} \cong 1.8$ and 2.3 Å, and $2a_1^2\ 1b_2^2\ 3a_1^2\ 1b_1^0\ (3p_x^1)_{Rydberg}\ (5a_1^2)_{H2}$ at larger than $R_{(NH)} \cong 2.3$ Å. In the electronic structure, $2a_1^2\ 1t_1^6\ (4s^1)_{Rydberg}$ represents $(NH_4^+)(e^-)_{4s}$, $2a_1^2\ 1b_2^2\ 3a_1^1\ 1b_1^2\ (5a_1^2)_{Rydberg}$ represents $[(NH_2^*)\ldots(H_2)]$, $2a_1^2\ 1b_2^2\ 3a_1^2\ 1b_1^0\ (4a_1^1)_{Rydberg}\ (5a_1^2)_{H2}$ represents $[(NH_2)\ldots(H_2^+)](e^-)_{3s}$, $2a_1^2\ 1b_2^2\ 3a_1^2\ 1b_1^0\ (5a_1^2\ 6a_1^1)_{H2}$ represents $(NH_2^+\ldots H_2^-)$, and $2a_1^2\ 1b_2^2\ 3a_1^2\ 1b_1^0\ (3p_x^1)_{Rydberg}\ (5a_1^2)_{H2}$ represents $[(NH_2^+)(e^-)_{3px} + H_2]$. Between $R_{(NH)} \cong 1.8$ and 2.3 Å, the dominant configuration represents $2a_1^2\ 1b_2^2\ 3a_1^2\ [(1\sigma)^2\ (1\sigma^*)^1]_{H2}$ which means the attractive interaction of $[NH_2^+\ldots H_2^-]$. When the internuclear distance between NH_2^+ and H_2^- become short, the attractive state emerging from an ion–ion pair $[NH_2^+ + H_2^-]$ diabatically correlates to NH_4. This state is diabatically bound due to the ion–ion electrostatic attraction. These dominant configurations are in accordance with the avoided curve crossings of Figure 4.

3.2 Potential Curves of H_3O Dissociating into its Asymptote

Geometric parameters at the equilibrium and transition states, the relative energies of H_3O dissociating into (H_2O + H) and (OH + H_2), and the ionization and excitation energies of H_3O, H_2O, OH, and H_2 are listed in Table 4. Our results for H_3O calculated by the SDCI, MP2, and CCSD(t) methods are in line with the experimental [10,37,40,49,84,85,93–95] and theoretical [43,44,46,47,87–92] values. Since the ground state of H_3O has an electron in a Rydberg 3s orbital, H_3O is a semi–ionic structure described as $(H_3O^+)(e^-)_{3s}$. At the equilibrium internuclear distance, $R_{(OH)eq}$ calculated with the SDCI and CCSD(t) methods are ≅ 1.022 and 1.020 Å, respectively. $R_{(OH)eq}$ of H_3O is longer than that [$R_{(OH)eq} \cong 0.962$ Å) of H_2O.

For the $^2A_1$ state of H_3O dissociating into (H_2O + H) and (OH + H_2), $R_{(OH)TS}$ at the SDCI level are ≅ 1.213 and ≅ 1.513 Å. The relative energy differences from the transition state to H_3O and (H_2O + H) are ≅ 0.12 and ≅ 0.97 eV, respectively. The energy differences from the transition state

to H_3O and [$OH(A^2\Sigma^+)$ + H_2] are ≅ 4.99 and ≅ 1.14 eV, respectively. The energy gaps between H_3O and (H_2O + H) and between H_3O and [$OH(A^2\Sigma^+)$ + $H_2(X^1\Sigma_g^+)$] are –0.86 and –3.85 eV, respectively. In the $^2B_1$ state of H_3O dissociating into (OH + H_2), $R_{(OH)eq}$ and $R_{(OH)TS}$ are ≅ 1.019 and ≅ 1.501 Å, respectively. The energy differences from the transition state to H_3O and [$OH(X^2\Pi)$ + $H_2(X^1\Sigma_g^+)$] are ≅ 5.02 and 7.18 eV, respectively. The energy gap of $^2B_1$ between H_3O and [$OH(X^2\Pi)$ + $H_2(X^1\Sigma_g^+)$] is –2.15 eV. Because the ground potential curve has a very low barrier, H_3O is very unstable. That is, the bond breaking takes place near the equilibrium geometry of H_3O. As a result, the existence of H_3O has not been observed experimentally.

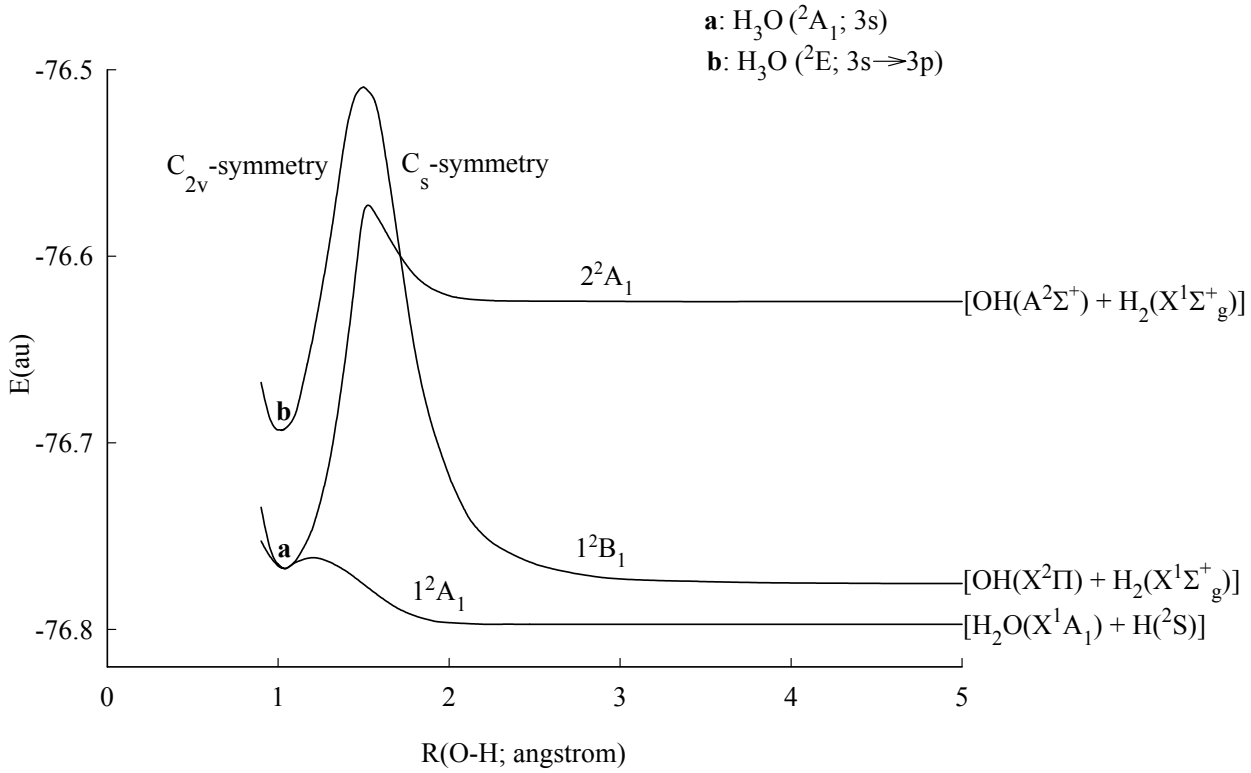

Figure 5. Potential energy curves for the $^2A_1$ and $^2B_1$ states of the Rydberg H_3O radical dissociating into (H_2O + H) and (OH + H_2) obtained with the SDCI level.

The ground potential energy curve of the H_3O radical dissociating into (H_2O + H) were calculated by Niblaeus *et al*. [46] and Luo and Jungen [49]. At the equilibrium geometry, the bond distances [$R_{(OH)eq}$] are ≅ 1.053 and ≅ 1.02 Å, respectively. The bond angles (∠HOH) are ≅ 101.8 and ≅ 106.9 degree, respectively. And the bond distance [$R_{(OH)TS}$] at the transition state is ≅ 1.248 Å. The barrier heights from the transition state to H_3O are ≅ 0.13 and ≅ 0.08 eV, respectively. The energy gaps between H_3O and (H_2O + H) calculated by CI and CEPA methods are –0.89 and –1.0 eV, respectively. Meanwhile, in investigations performed by Melton and Joy [37], the structure of H_3O has a planar geometry. The bond distance [$R_{(OH)eq}$] is ≅ 1.053 Å. They predicted that the H_3O radical is stable relative to (H_2O + H).

As shown in Table 4, our results for the formation of H_3O from its asymptotic products are

slightly endothermic by 0.12 eV. By the weak interaction between the nuclear and a Rydberg electron, the geometric structure of H_3O is similar to that of H_3O^+. The ionization and excitation energies of H_3O are relatively low. That is, the excitation energies of the Rydberg transitions (3s→higher orbitals) should be lower than the ionization potential of ≅ 5.30 eV. On the other hand, the ionization potential and proton affinity of H_2O are ≅ 12.54 and ≅ 7.32 eV at the SDCI level, respectively. The ionization energy (≅ 12.71 eV) and electron affinity (≅ 1.81 eV) of OH are relatively large. The ionization potential and electron affinity of H_2 are ≅ 15.43 and ≅ 1.38 eV, respectively. The potential energy curves for the $^2A_1$ and $^2B_1$ states of the Rydberg H_3O radical dissociating into its dissociation product are drawn in Figure 5. The potential energy curves for the dissociation reactions of (H_2O + H) and (OH + H_2) are slightly endothermic. The energy gap between [$OH(X^2\Pi_1)$ + $H_2(X^1\Sigma_g^+)$] and [$H_2O(X^1A_1)$ + $H(^2S)$] asymptotes is ≅ 0.66 eV. The energy gap between [$OH(X^2B_1)$ + $H_2(X^1\Sigma_g^+)$] and [$OH(A^2\Sigma^+)$ + $H_2(X^1\Sigma_g^+)$] asymptotes is ≅ 4.0 eV.

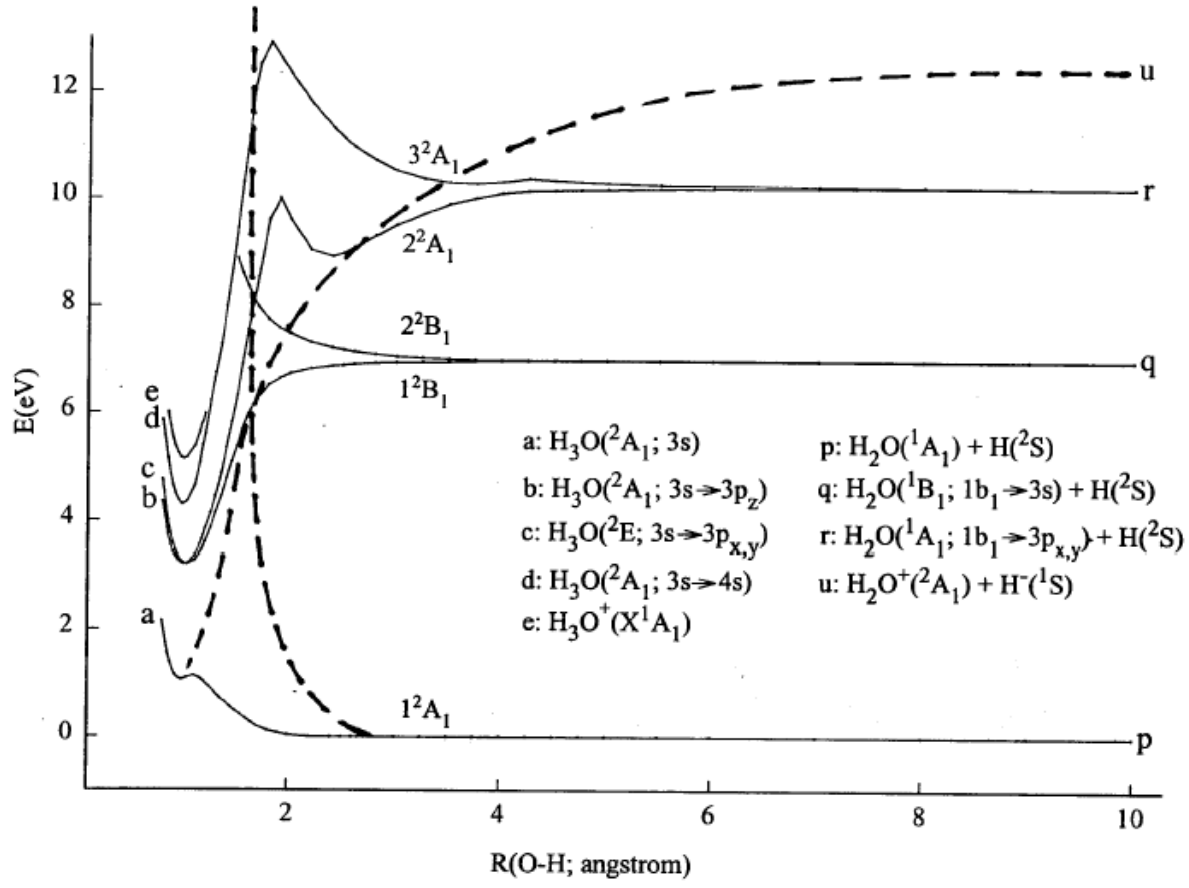

Figure 6. Adiabatic potential energy curves for the ground and excited states of the Rydberg H_3O radical dissociating into (H_2O + H). Broken lines indicate estimated diabatic potential curves.

The thermodynamic cycle based on the experimental results was drawn by Williams and Porter [10]. The energies of H_3O dissociating into (H_2O + H) in the Na and K target atoms are –1.12±0.07 and –1.57±0.07 eV, respectively. The fragmentation energies of the H_3O radical dissociating into (OH + H_2) in the Na and K target atoms are –0.54±0.03 and –0.74±0.04 eV, respectively. The

vertical electron affinities of H_3O^+ in the Na and K targets are 5.3 and 5.0 eV, respectively. The relative energy level of the (H_2O + H) asymptote is 15 kcal/mol stable with respect to that of the (OH + H_2) asymptote. A metastable state of H_3O with a lifetime greater than 10^{-7} sec was not obtained. ESR spectrum of matrix–stabilized hydronium H_3O is obtained by Martin and Swift [38]. H_3O is stable by bond dissociation energy of 7 kcal/mol relative to (H_2O +H). In the experiments performed by Gellene and Porter [40], the H_3O radical is obtained from an electron capture process of their parent ion in a collision with a beam of metal atoms. The apparent electron affinity determined by fragmentation energy is 3.88 eV. The ionization potential and transition energy (3s→3p) of D_3O are estimated to be 4.3±0.1 and 1.6 eV, respectively. Raynor *et al*. [47] have calculated transition energy (3s→3p) to be the range of 1.87 – 2.25 eV for H_3O and the ionization potential of 4.68 eV.

Under the C_{2v}–symmetry constraints, the potential energy curves for the ground and low lying excited states of H_3O dissociating into (H_2O + H) and (OH + H_2) are drawn in Figure 6 and 7, respectively. And they are labeled as 1^2A_1, 2^2A_1, 3^2A_1, 4^2A_1, 1^2B_1, and 2^2B_1, respectively. The ground $^2A_1$ state of H_3O correlates with a repulsive state emerging from an antibonding interaction of the [$H_2O(^1A_1)$ + $H(^2S)$] and [$OH(A^2\Sigma^+)$ + $H_2(X^1\Sigma_g^+)$] asymptote. It is made by an avoided curve crossing between the dissociative diabatic state of the Rydberg [$(H_3O^+)(e^-)_{3s}$] radical and the repulsive diabatic state emerging from the [$H_2O(^1A_1)$ + $H(^2S)$] and [$OH(A^2\Sigma^+)$ + $H_2(X^1\Sigma_g^+)$] asymptotes. This curve is quasibound, which means that its equilibrium energy is higher than that of the dissociation asymptote of its dissociation products. The barrier height and potential well are very low and shallow, respectively. The potential curve has an energy barrier near the equilibrium geometry of H_3O. In the ground potential energy curve, the maximum position [$R_{(OH)} \cong 1.213$ Å] of the transition state is located out of line of those of the first and higher excited states.

In H_3O dissociating into (H_2O + H) of the Figure 6, the ground Rydberg H_3O radical diabatically dissociates into the first excited [$H_2O(^1A_1; 1b_1\rightarrow 3p_{x,y})$ + $H(^2S)$] and the ion–ion pair [$H_2O^+(^2A_1)$ + $H^-(^1S)$] asymptotes. In the second dissociation path, one electron jumps from the $1b_1$ orbital of H_2O to the 1s orbital of H. The ion pair has strongly attractive ionic character as an ion approaches to the other. By the avoided curve crossing between strongly attractive ionic states emerging from [$H_2O^+(^2A_1)$ + $H^-(^1S)$] and the repulsive diabatic state from [$H_2O(^1A_1)$ + $H(^2S)$], the potential energy barrier of the ground $^2A_1$ state is shifted to the equilibrium geometry of H_3O. The barrier height is found to be low. All potential curves of the excited states formed by the curve crossings are bound between $R_{(OH)} \cong 2.0$ Å and ≅ 4.0 Å. In the first 2^2A_1 state, the curve crossings between the dissociative diabatic excited states of [$(H_3O^+)(e^-)_{Rydberg}$] and the repulsive diabatic states from the antibonding interaction of [$H_2O(^1A_1; 1b_1\rightarrow 3p_{x,y})$ + $H(^2S)$] are found between $R_{(OH)} \cong 1.5$ Å and ≅ 4.0 Å. Because of the energy barrier formed by the curve crossing, the potential curve is bound around $R_{(OH)} \cong 2.5$ Å. The 3^2A_1 state emerging from the [$H_2O(^1A_1; 1b_1\rightarrow 3p_{x,y})$ + $H(^2S)$] asymptote is diabatically repulsive. By the avoided curve crossings, this state is shallowly bound around

$R_{(OH)} \cong 3.75$ Å. The first excited ^2E state emerging from H_3O ($3s \rightarrow 3p_{x,y}$) directly correlates with an attractive state from the $[H_2O(^1B_1;1b_1 \rightarrow 3s) + H(^2S)]$ asymptote.

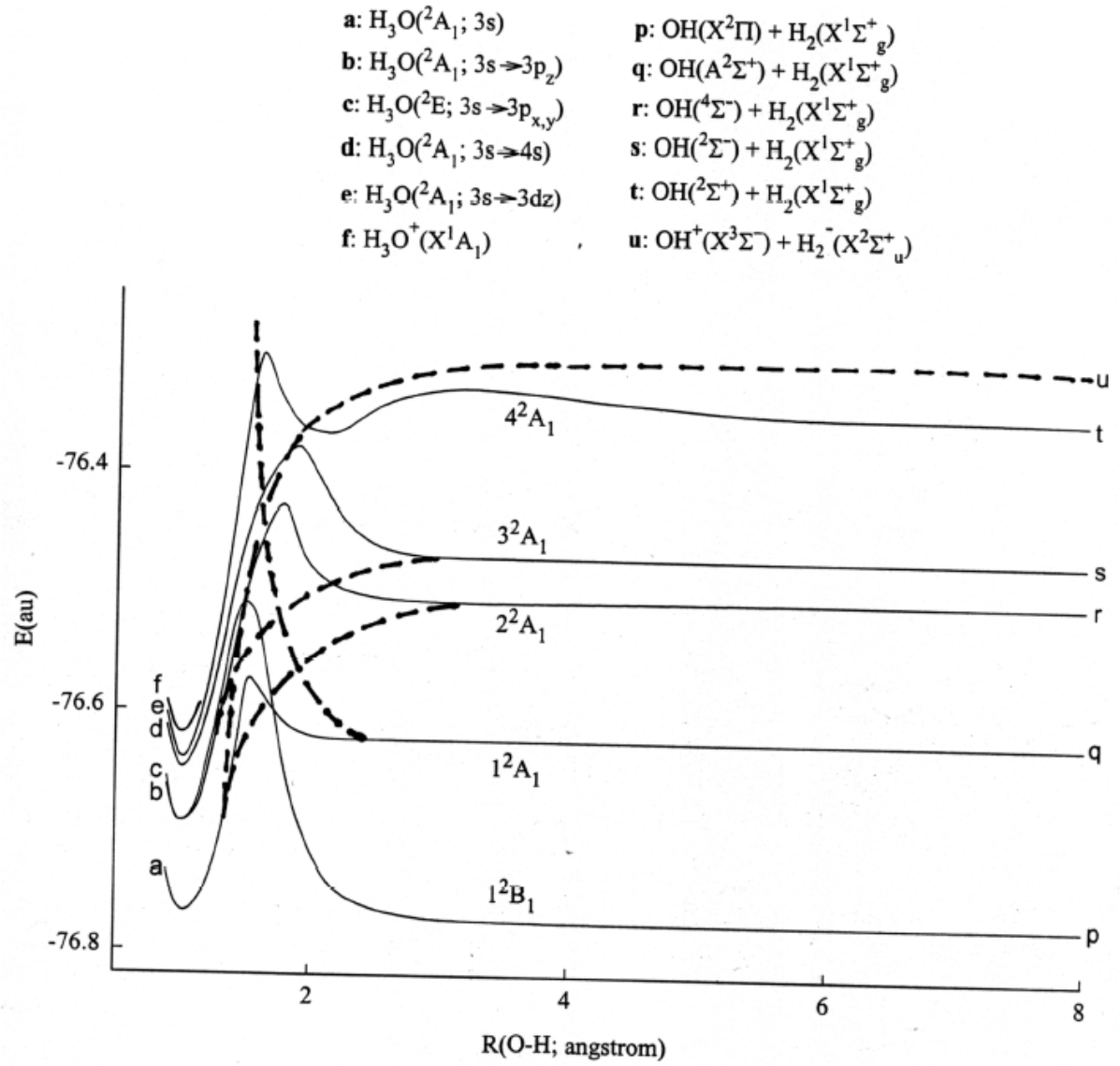

Figure 7. Avoided curve crossings for the $^2A_1$states of the Rydberg H_3O radical dissociating into ($OH + H_2$). Broken lines indicate estimated diabatic potential curves.

In H_3O dissociating into ($H_2O + H$) of the Figure 7, the ground Rydberg H_3O radical diabatically dissociates into the first excited $[OH(A^2\Sigma^+) + H_2(X^1\Sigma_g^+)]$ and the ion–ion pair $[OH^+(X^3\Sigma^-) + H_2^-(X^2\Sigma_u^+)]$ asymptotes. In the second dissociation path, one electron also jumps from the $1\pi^3$ orbital of OH to the $1\sigma^*$ orbital of H_2. All potential energy curves emerging from the antibonding interaction of the ($OH^* + H_2$) asymptotes are diabatically repulsive, while a potential energy curve emerging from the $[OH^+(X^3\Sigma^-) + H_2^-(X^2\Sigma_u^+)]$ asymptote is diabatically attractive. At shorter than $R_{(OH)} \cong 1.8$ Å, the avoided curve crossings between the dissociative diabatic states of $[(H_3O^+)(e^-)_{Rydberg}]$ and the repulsive diabatic states from ($OH^* + H_2$) are occurred. At larger than $R_{(OH)} \cong 1.8$ Å, the curve crossings between the diabatically attractive diabatic state of $[OH^+(X^3\Sigma^-) + H_2^-(X^2\Sigma_u^+)]$ and the

diabatically repulsive diabatic states of (OH^* + H_2) are found. As a result, two potential barriers in the 4^2A_1 state are formed by two kinds of curve crossings. By the avoided curve crossings, the potential energy curve of the 4^2A_1 state is bound between $R_{(OH)} \cong 2.3$ and 5.8 Å. Meanwhile, in the excited 2^2A_1 and 3^2A_1 states, a potential energy barrier is found at $R_{(OH)} \cong 1.8$ Å. That is, the barriers of the excited 2^2A_1 and 3^2A_1 states are coupled by strongly avoided curve crossings between strongly attractive ionic states emerging from ($OH^+ + H_2^-$) and the repulsive diabatic state from (OH^* + H_2). For the $^2B_1$ states of H_3O dissociating into (OH + H_2), the 1^2B_1 state emerging from [$OH(X^2\Pi)$ + $H_2(X^1\Sigma_g^+)$] asymptote correlates to the ^2E excited state of H_3O. It is also made by an avoided curve crossing between the dissociative diabatic state of the Rydberg [$(H_3O^+)(e^-)_{Rydberg}$] radical and the repulsive diabatic state emerging from the (OH^* + H_2) asymptote.

Table 5. Contributions of the dominant configuration for the low lying Rydberg $^2A_1$ states along the H_3O radical dissociating into (H_2O + H). 22221 denotes $2a_1^2\ 1e^4\ 3a_1^2\ 4a_1^1$ configuration. The core part is abbreviated and a degenerated orbital of $1e^4$ is indicated as 22.

$R_{(OH)}$ (Å)	1^2A_1		2^2A_1		3^2A_1	
0.8	22221	0.9982	22220010	0.9989	222200010	0.9997
0.9	22221	0.9970	22220010	0.9976	222200010	0.9990
1.0	22221	0.9957	22220010	0.9959	222200010	0.9987
1.2	22221	0.9924	22220010	0.9924	222200100	0.9972
1.4	22221	0.9893	22220010	0.9827	222200100	0.9914
1.6	22221	0.9800	22220010	0.9681	222200100	0.9837
1.8	22221	0.9819	22220010	0.9322	222200100	0.9261
2.0	22221	0.9838	22220010	0.8301	222110100	0.7155
2.2	22221	0.9851	22210002	0.4418	222110001	0.6599
			22220010	0.2301		
2.5	22221	0.9864	22210002	0.4875	222110001	0.6856
			22220010	0.2801		
3.0	22221	0.9873	22210002	0.5046	222110001	0.7009
			22211001	0.3236		
3.5	22221	0.9886	22210002	0.5375	222110001	0.6714
			22211001	0.4036		
4.0	22221	0.9890	22210002	0.6009	222100002	0.7009
			22211001	0.4460		
5.0	22221	0.9893	22211001	0.4915	222110001	0.5805
6.0	22221	0.9896	22211001	0.5458	222110001	0.6164
7.0	22221	0.9898	22211001	0.5609	222110001	0.6865
8.0	22221	0.9990	22211001	0.5720	222110001	0.6923
10.0	22221	0.9993	22211001	0.5817	222110001	0.7715

Adiabatic potential energy curves of the dissociation of H_3O into (H_2O + H) have been investigated by some groups [44,46,49]. According to their curves, the ground $^2A_1$ state surface along the OH bond rupture has a very low potential energy barrier. In the result of Luo and Jungen [49], a barrier height is found to be ≅ 0.08 eV. Particularly, around $R_{(OH)} \cong 3.0$ Å, the curve is also bound shallowly. In the results of Niblaeus *et al*. [46], a barrier of ≅ 0.13 eV is found at $R_{(OH)} \cong 1.248$ Å. The potential barrier is found to be sensitive to the diffuse basis set. They concluded that the origin of the barrier is a curve crossing between a repulsive state and an attractive Rydberg state. But, the avoided curve crossings have not been represented clearly.

Table 6. Contributions of the dominant configuration for two $^2A_1$ states along the H_3O radical dissociating into (OH + H_2). Configuration of $2a_1^2\ 1e^4\ 3a_1^2\ 4a_1^1$ denotes 2421. The core part is abbreviated.

$R_{(OH)}$ (Å)	1^2A_1		2^2A_1	
0.8	242100	0.9951	24200001	0.9596
0.9	242100	0.9922	24200001	0.9486
1.0	242100	0.9892	24200001	0.9379
1.1	242100	0.9821	24200001	0.9185
1.2	222210	0.9736	22112001	0.8951
1.4	222210	0.8967	22112001	0.7825
1.5	222210	0.7749	22112001	0.5976
			22110021	0.3858
1.6	222201	0.6879	22211001	0.4786
			22110021	0.5053
1.8	222201	0.6709	22211001	0.3520
			22110021	0.6472
2.0	212202	0.7842	22211001	0.2308
			22110021	0.7354
2.1	212202	0.8401	22111002	0.5650
2.2	212202	0.9083	22111002	0.5916
2.3	212202	0.9187	22111002	0.6447
2.5	212202	0.9241	22111002	0.6772
3.0	212202	0.9329	22111002	0.7270
3.5	212202	0.9381	22111002	0.7973
4.0	212202	0.9416	22111002	0.8377
5.0	212202	0.9426	22111002	0.8539
6.0	212202	0.9434	22111002	0.8580
7.0	212202	0.9442	22111002	0.8603
8.0	212202	0.9446	22111002	0.8699

Here, it is important thing to investigate the characteristically avoided curve crossings of the potential curves for the dissociation of H_3O into its product asymptotes. The potential curves for the dissociation of [(AH_a^+)(e^-)$_{Rydberg}$] into its products are formed by two kinds of the avoided curve crossings. One is occurred between the dissociative diabatic states emerging from [(AH_a^+)(e^-)$_{Rydberg}$] and the repulsive diabatic states from (AH_b^* + H_c). The other is occurred between the repulsive diabatic states emerging from (AH_b^* + H_c) and the attractively ionic diabatic state from the ion–ion pair (AH_b^+ + H_c^-) asymptote. To understand the avoided curve crossing, we have analyzed the contributions of the dominant configuration to the total wave functions of the $^2A_1$ states and listed them in Tables 5 and 6.

The dominant configuration for the ground $^2A_1$ state is [core]$2a_1^2\ 1e^4\ 3a_1^2\ 4a_1^1$ at the H_3O structure, [core]$2a_1^2\ 1b_2^2\ 3a_1^2\ 1b_1^2\ (4a_1^1)_H$ at the (H_2O + H) asymptote, and [core]$2\sigma^2\ 3\sigma^1\ 1\pi_x^2\ 1\pi_y^2\ (4\sigma^2)_{H2}$ at the (OH + H_2) asymptote. $2a_1^2\ 1e^4\ 3a_1^2$ is an electronic configuration of H_3O^+. $4a_1^1$ indicates an electron of the Rydberg 3s orbital having a H_3O^+ structure as a core. The electronic structure of H_3O is represented to be [(H_3O^+)(e^-)$_{3s}$]. Along OH bond rupture, the $4a_1$ orbital is nonbonding, *i.e.*, a character of 1s of H. $4a_1^1$ indicates one electron in the 1s orbital of H. That is, the configuration of $2a_1^2\ 1e^4\ 3a_1^2\ (1s^1)_H$ at $R_{(OH)}$=10.0 Å indicates the antibonding pair [$H_2O(^1A_1)$ + $H(^2S)$] asymptote. As a result, the dominant configuration of the ground $^2A_1$ state interconnecting the H_3O structure with the (H_2O + H) asymptote does not change from short internuclear distance to

long. Meanwhile, along OH–H_2 bond rupture, the $(4\sigma^2)_{H2}$ orbital is a bonding character of $1\sigma^2$ of H_2. 1e orbital of H_3O separates into two orbitals ($1\pi_x$, $1\pi_y$) in OH. Therefore, the configuration of $2\sigma^2\ 3\sigma^1\ 1\pi_x^2\ 1\pi_y^2\ (4\sigma^2)_{H2}$ at $R_{(OH)}$=8.0 Å indicates the antibonding pair [$OH(A^2\Sigma^+)$ + $H_2(X^1\Sigma_g^+)$] asymptote.

For the dissociation of H_3O into (H_2O + H), the ground $(H_3O^+)(e^-)_{3s}$ radical diabatically correlates into the [$H_2O(^1A_1;\ 1b_1\rightarrow 3p_{x,y})$ + $H(^2S)$] and [$H_2O^+(^2A_1)$ + $H^-(^1S)$] asymptotes. In Table 5, the dominant configurations of the [$H_2O(^1A_1;\ 1b_1\rightarrow 3p_{x,y})$ + $H(^2S)$] and [$H_2O^+(^2A_1)$ + $H^-(^1S)$] asymptotes are <u>22211001</u> and <u>22210002</u>, respectively. In the diabatic dissociation of H_3O into [$H_2O(^1A_1;\ 1b_1\rightarrow 3p_{x,y})$ + $H(^2S)$], the contribution for the configuration of <u>22211001</u> begins to appear the first excited $^2A_1$ state at $R_{(OH)}$ = 3.0 Å and the contribution of it increases with internuclear distance. From $R_{(OH)}$ = 5.0 Å it become a dominant configuration in the first $^2A_1$ state. In the diabatic dissociation of H_3O into the ion–ion pair [$H_2O^+(^2A_1)$ + $H^-(^1S)$] asymptote, the contribution for the configuration of <u>22210002</u> represents the first excited $^2A_1$ state from $R_{(OH)}$ = 2.2 Å to 4.0 Å. Around $R_{(OH)}$ = 4.0 Å, the contribution represents the second excited $^2A_1$ state. This configuration can be strongly attractive ion character as an ion approaches to the other. Two attractive diabatic characters greatly influence the curve crossing, that is, the contributions of those characters are larger than that of the repulsive character. As the result, the potential energy barrier of the ground $^2A_1$ state is shifted to the equilibrium geometry of H_3O. And the barrier height appears to be low.

In the excited 2^2A_1 state, the dominant configuration is $2a_1^2\ 1e^4\ 3a_1^2\ (3p_z)^1_{Rydberg}$ at shorter than $R_{(OH)} \cong$ 1.1 Å, $2a_1^2\ 1b_2^2\ 3a_1^2\ 1b_1^2\ (3p_z)^1_{Rydberg}$ between $R_{(OH)} \cong$ 1.2 and ≅2.1 Å, $2a_1^2\ 1b_2^2\ 3a_1^2\ 1b_1^1\ (1s)^2_H$ between $R_{(OH)} \cong$ 2.2 and ≅ 4.5 Å, and $2a_1^2\ 1b_2^2\ 3a_1^2\ 1b_1^1\ (3p_{x,y})^1_{Rydberg}\ (1s)^1_H$ at larger than $R_{(OH)} \cong$ 4.5 Å. In the dissociation of H_3O into (H_2O + H), $2a_1^2\ 1e^4\ 3a_1^2\ (3p_z)^1_{Rydberg}$ at shorter than $R_{(OH)} \cong$ 1.1 Å represents the $(H_3O^+)(e^-)3p_z$ structure, $2a_1^2\ 1b_2^2\ 3a_1^2\ 1b_1^2\ (3p_z)^1_{Rydberg}$ between $R_{(OH)} \cong$ 1.2 and ≅ 2.1 Å represents $(H_2O\ldots H^+)(e^-)3p_z$, $2a_1^2\ 1b_2^2\ 3a_1^2\ 1b_1^1\ (1s)^2_H$ between $R_{(OH)} \cong$ 2.2 and ≅ 4.5 Å represents $(H_2O^+\ldots H^-)$, and $2a_1^2\ 1b_2^2\ 3a_1^2\ 1b_1^1\ (3p_{x,y})^1_{Rydberg}\ (1s)^1_H$ at larger than $R_{(OH)} \cong$ 4.5 Å represents $[(H_2O^+)(e^-)3p_{x,y}$ + H]. More interestingly, the 2^2A_1 state between $R_{(OH)} \cong$ 2.2 and ≅ 4.5 Å has a dominant configuration of $2a_1^2\ 1b_2^2\ 3a_1^2\ 1b_1^1\ (1s)^2_H$ which means an ion–ion interaction structure as $(H_2O^+\ldots H^-)$. Here one electron jumped from the Rydberg $3p_z$ orbital of H_2O to the 1s orbital of H.

The dominant configuration of the 3^2A_1 state is $2a_1^2\ 1e^4\ 3a_1^2\ (4s)^1_{Rydberg}$ at shorter than $R_{(OH)} \cong$ 1.1 Å, $2a_1^2\ 1b_2^2\ 3a_1^2\ 1b_1^2\ (3p_z)^1_{Rydberg}$ between $R_{(OH)} \cong$ 1.2 and ≅ 2.1 Å, $2a_1^2\ 1b_2^2\ 3a_1^2\ 1b_1^1\ (3p_{x,y})^1_{Rydberg}\ (1s)^1_H$ between $R_{(OH)} \cong$ 2.2 and ≅ 3.8 Å, $2a_1^2\ 1b_2^2\ 3a_1^2\ 1b_1^1\ (1s)^2_H$ between $R_{(OH)} \cong$ 3.8 and ≅ 4.5 Å, and $2a_1^2\ 1b_2^2\ 3a_1^2\ 1b_1^1\ (3p_{x,y})^1_{Rydberg}\ (1s)^1_H$ at larger than $R_{(OH)} \cong$ 4.5 Å. In the electronic structure, $2a_1^2\ 1e^4\ 3a_1^2\ (4s)^1_{Rydberg}$ represents $(H_3O^+)(e^-)_{4s}$, $2a_1^2\ 1b_2^2\ 3a_1^2\ 1b_1^2\ (3p_z)^1_{Rydberg}$ represents $[(H_2O)\ \ldots(H^+)](e^-)3p_z$, $2a_1^2\ 1b_2^2\ 3a_1^2\ 1b_1^1\ (1s)^2_H$ represents $(H_2O^+\ldots H^-)$, and $2a_1^2\ 1b_2^2\ 3a_1^2\ 1b_1^1\ (3p_{x,y})^1_{Rydberg}\ (1s)^1_H$ represents $[(H_2O^+)(e^-)_{3s}$ + H]. Around $R_{(OH)} \cong$ 4.0 Å, the dominant

configuration represents $2a_1^2\ 1b_2^2\ 3a_1^2\ 1b_1^1\ (1s)^2_H$ which means the attractive interaction of $[H_2O^+ \ldots H^-]$. The changes of these configurations are in accordance with the potential energy curves in Figure 6.

For the dissociation of H_3O into (OH + H_2), the ground $^2A_1$ state of the $(H_3O^+)(e^-)_{3s}$ radical diabatically correlates into the $[OH(^4\Sigma^-) + H_2(X^1\Sigma_g^+)]$ and $[OH^+(X^3\Sigma^-) + H_2^-(X^2\Sigma_u^+)]$ asymptotes. The dominant configurations of $[OH(^4\Sigma^-) + H_2\ (X^1\Sigma_g^+)]$ and $[OH^+(X^3\Sigma^-) + H_2^-(X^2\Sigma_u^+)]$ are 221112 as a [core] $2\sigma^2\ 3\sigma^2\ 1\pi_x^1\ 1\pi_y^1\ 4\sigma^1\ (1\sigma^2)_{H2}$ configuration and 221121 as [core] $2\sigma^2\ 3\sigma^2\ 1\pi_x^1\ 1\pi_y^1\ [(1\sigma)^2\ (1\sigma^*)^1]_{H2}$, respectively. In diabatic dissociation of H_3O into $[OH(^4\Sigma^-) + H_2\ (X^1\Sigma_g^+)]$, the contribution for the configuration of 221112 begins to appear the 2^2A_1 state at $R_{(OH)}$ = 2.1 Å and the contribution of it increases with internuclear distance. In diabatic dissociation of H_3O into $[OH^+(X^3\Sigma^-) + H_2^-(X^2\Sigma_u^+)]$, the contribution for the configuration of 221121 represents the 2^2A_1 state from $R_{(OH)}$ = 1.5 to 2.0 Å. This configuration can be strongly attractive ion character as an ion approaches to the other. The attractive diabatic character greatly influences on the curve crossing, that is, the contribution of this character is larger than that of the repulsive character.

In the excited 2^2A_1 state, the dominant configuration is $2a_1^2\ 1e^4\ 3a_1^2\ (3p_z)^1_{Rydberg}$ at shorter than $R_{(OH)} \cong$ 1.1 Å, $2\sigma^2\ 3\sigma^2\ 1\pi_x^1\ 1\pi_y^1\ (4\sigma)^2\ (3p_z)^1_{Rydberg}$ between $R_{(OH)} \cong$ 1.2 and $\cong$ 1.5 Å, $2\sigma^2\ 3\sigma^2\ 1\pi_x^1\ 1\pi_y^1\ [(1\sigma)^2\ (1\sigma^*)^1]_{H2}$ between $R_{(OH)} \cong$ 1.5 and $\cong$ 2.0 Å, and $2\sigma^2\ 3\sigma^2\ 1\pi_x^1\ 1\pi_y^1\ 4\sigma^1\ (1\sigma^2)_{H2}$ at larger than $R_{(OH)} \cong$ 2.1 Å. That is, at shorter than $R_{(OH)} \cong$ 1.1 Å, $2a_1^2\ 1e^4\ 3a_1^2\ (3p_z)^1_{Rydberg}$ represents the $(H_3O^+)(e^-)_{3pz}$ structure, $2\sigma^2\ 3\sigma^2\ 1\pi_x^1\ 1\pi_y^1\ (4\sigma)^2\ (3p_z)^1_{Rydberg}$ between $R_{(OH)} \cong$ 1.2 and $\cong$ 1.5 Å represents $(HO \ldots H_2)^+(e^-)3p_z$, $2\sigma^2\ 3\sigma^2\ 1\pi_x^1\ 1\pi_y^1\ [(1\sigma)^2\ (1\sigma^*)^1]_{H2}$ between $R_{(OH)} \cong$ 1.5 and $\cong$ 2.0 Å represents $(HO^+ \ldots H_2^-)$, and $2\sigma^2\ 3\sigma^2\ 1\pi_x^1\ 1\pi_y^1\ 4\sigma^1\ (1\sigma^2)_{H2}$ at larger than $R_{(OH)} \cong$ 2.1 Å represents $[OH(^4\Sigma^-) + H_2(X^1\Sigma_g^+)]$. More interestingly, the 2^2A_1 state between $R_{(OH)} \cong$ 1.5 and $\cong$ 2.0 Å has a dominant configuration of $2\sigma^2\ 3\sigma^2\ 1\pi_x^1\ 1\pi_y^1\ [(1\sigma)^2\ (1\sigma^*)^1]_{H2}$ which means an ion–ion interaction structure as $(HO^+ \ldots H_2^-)$. Here one electron jumped from the Rydberg $3p_z$ orbital of OH to the $[(1\sigma^*)^1]_{H2}$ orbital of H_2. Therefore, this state has strongly attractive ion character. The changes of these configurations are in accordance with the potential energy curves in Figure 7.

As shown in Figure 6 and 7, in the H_3O radical dissociating into (H_2O + H), the potential energy barrier is formed by two avoided curve crossings between two attractive diabatic states emerging from $[H_2O(^1A_1;1b_1 \rightarrow 3p_{x,y}) + H(^2S)]$ and $[H_2O^+(^2A_1) + H^-(^1S)]$ and a repulsive state from an antibonding interaction of $[H_2O(^1A_1) + H(^2S)]$. Two attractive characters from $[H_2O(^1A_1;\ 1b_1 \rightarrow 3p_{x,y}) + H(^2S)]$ and $[H_2O^+(^2A_1) + H^-(^1S)]$ greatly influence on the curve crossing. In the H_3O radical dissociating into (OH + H_2), the ground $^2A_1$ state of the Rydberg H_3O radical diabatically dissociates into the $[OH(^4\Sigma^-) + H_2(X^1\Sigma_g^+)]$ and $[OH^+(X^3\Sigma^-) + H_2^-(X^2\Sigma_u^+)]$ asymptotes. When the internuclear distance between OH^+ and H_2^- become short, the attractive state emerging from the ion–ion pair diabatically correlates with H_3O. This state is diabatically bound due to the ion–ion electrostatic attraction. As a result, the maximum position of the ground potential barrier formed by

the avoided curve crossing is located out of line of those of the excited potential energy curves.

4 CONCLUSIONS

We have calculated the state–to–state correlation curves for the dissociation reaction of the Rydberg $[(AH_a^+)(e^-)_{Rydberg}]$ radical into $(AH_b + H_c)$ under the C_{2v}– and C_{3v}–symmetry constraints and analyzed the contributions of the dominant configurations for the ground and low lying excited states. The ground potential curve has a relatively low potential energy barrier and the maximum position of the potential barrier exists near the equilibrium geometry of AH_a. The potential barriers are formed by two kinds of the avoided curve crossings. One is occurred between the dissociative diabatic states emerging from $[(AH_a^+)(e^-)_{Rydberg}]$ and the repulsive diabatic states from an antibonding interaction of $[AH_b^*(n\rightarrow 3s) + H_c]$. At shorter than $R_{(AH)} \cong 2.0$ Å, the curve crossing are represented mainly. The other is occurred between the repulsive diabatic states emerging from $[AH_b^*(n\rightarrow 3s) + H_c]$ and the attractively ionic diabatic states from the $[AH_b^+ + H_c^-]$ asymptotes. The curve crossings are also represented at larger than $R_{(AH)} \cong 2.0$ Å. When AH^+ and H_2^- ions approach to each other from infinite separation, there exists strong electrostatic attraction between two ions. The attractive state emerging from the cation–anion pair is bound strongly. These curve crossings are greatly influenced by the attractive characters from the cation–anion pair $[AH_b^+ + H_c^-]$ asymptote. In the excited curves, the potential energy curves are also shallowly bound. The potential wells are also formed by the avoided curve crossings between the dissociative diabatic excited states of $[(AH_a^+)(e^-)_{Rydberg}]$ and the repulsive diabatic states from the antibonding interactions of $[AH_b^*(n\rightarrow 3s) + H_c]$.

In AH_a dissociating into $(AH_b + H_c)$, each state of AH_a corresponds to each state emerging from $(AH_b + H_c)$. In the correlation curve if the potential energy barriers of the states are determined by the avoided curve crossings, the barrier height should be high and the maximum position should be located at middle place between $[(AH_a^+)(e^-)_{Rydberg}]$ and $(AH_b + H_c)$. But, the potential barrier heights of the excited states are appeared to be low and the barriers are located near the equilibrium geometry of AH_a. In $[(AH_a^+)(e^-)_{Rydberg}]$ dissociating into $(AH_b^+ + H_c^-)$, this state is diabatically bound due to the strongly cation–anion electrostatic attraction. As the result, the position of the avoided curve crossing is shifted to the equilibrium geometry of $[(AH_a^+)(e^-)_{Rydberg}]$ and the maximum position of potential barrier of the ground state formed by the avoided curve crossing is located out of line of those of the excited potential energy curves. The attractive diabatic characters emerging from $(AH_b^+ + H_c^-)$ may be played an important role in the state–to–state correlation curves for the dissociation reaction.

For NH_4 dissociating into $(NH_3 + H)$, the energy barrier height of $^2A_1$ from the transition state to NH_4 is ≅ 0.83 eV. For NH_4 dissociating into $(NH_2 + H_2)$, the barrier heights of $^2A_1$ and $^2B_1$ from the transition state to NH_4 are ≅ 3.59 and 2.96 eV, respectively. For the $^2A_1$ state of H_3O dissociating

into (H_2O + H), the energy difference from the transition state to H_3O is ≅ 0.12 eV. In H_3O dissociating into (OH + H_2), the energy differences of the $^2A_1$ and $^2B_1$ states from the transition state to H_3O are ≅ 4.99 and ≅ 5.02 eV, respectively. Because the equilibrium geometric structure of H_2F have not been optimized, the potential barriers for H_2F dissociating into its asymptotes are nearly zero. Therefore, along the A–H bond rupture, the ground states of NH_4, H_3O, and H_2F have energy barriers of ≅ 0.83, 0.12, and 0 eV, respectively. The relative potential barriers from NH_4 to H_2F decrease stepwise. Because the relative potential barrier of NH_4 is largest than those of H_3O and H_2F, the existence of NH_4 in cluster has been observed experimentally. But, H_3O and H_2F have been scarcely observed.

Acknowledgment

We thank the Korea Research Foundation (KRF) for supporting this work through the Basic Science Research Institute program (KRF–2002–015–CP0161). The author thanks Dr. Hosung Sun for valuable helps.

5 REFERENCES

[1] F. Misaizu, P. L. Houston, N. Nishi, H. Shinohara, T. Kondow, and K. Kinoshita,. *J. Chem. Phys*. **1993**, *98*, 336.
[2] L. A. Posey, R. D. Guettler, N. J. Kirchner, and R. N. Zare, *J. Chem. Phys*. **1994**, *101*, 3772.
[3] S. A. Buzza, S. Wei, J. Purnell, and A. W. Castleman, Jr., *J. Chem. Phys*. **1995**, *102*, 4832.
[4] F. Fuke, R. Takasu, and F. Misaizu, *Chem. Phys. Lett*. **1994**, 229, 597; K. Fuke, and R. Takasu, *Bull. Chem. Soc. Jpn*. **1995**, *68*, 3309.
[5] G. Herzberg, *Faraday Discuss. Chem. Soc*. **1981**, *71*, 165.
[6] O. S. Mortensen, B. R. Henry, and M. A. Mohammadi, *J. Chem. Phys*. **1981**, *75*, 4800.
[7] S. T. Ceyer, P. W. Tiedemann, B. H. Mahan, and Y. T. Lee, *J. Chem. Phys*. **1979**, *70*, 14.
[8] A. Schuster, *Rep. Brit. Assoc*. 1872, pp.38.
[9] H. Schüler, A. Michel, and A. E. Grün, *Z. Naturforsch*. **1955**, *10a*, 1.
[10] B. W. Williams and R. F. Porter, *J. Chem. Phys*. **1980**, *73*, 5598.
[11] G. I. Gellene, D. A. Cleary, and R. F. Porter, *J. Chem. Phys*. **1983**, *77*, 3471.
[12] G. Herzberg and J. T. Hougen, *J. Mol. Spectrosc*. **1983**, *97*, 430.
[13] E. A. Whittaker, B. J. Sullivan, G. C. Bjorklund, H. R. Wendt, and H. E. Hunziker, *J. Chem. Phys*. **1984**, *80*, 961.
[14] J. K. G. Watson, *J. Mol. Spectrosc*. **1984**, *103*, 125; *J. Mol. Spectrosc*. **1984**, *107*, 124.
[15] F. Alberti, K. P. Huber, and J. K. G. Watson, *J. Mol. Spectrosc*. **1984**, *107*, 133.
[16] R. Signorell, H. Palm, and F. Merkt, *J. Chem. Phys*. **1997**, *106*, 6523.
[17] F. Misaizu, K. Tsukamoto, M. Sanekata, and K. Fuke, *Chem. Phys. Lett*. **1992**, *188*, 241.
[18] I. V. Hertel, C. Hüglin, C. Nitsch, and C. P. Schultz, *Phys. Rev. Lett*. **1991**, *67*, 1767.
[19] E. Kariv–Miller, C. Nanjundiah, J. Eaton, and K. E. Swenson, *J. Electroanal. Chem*. **1984**, *167*, 141.
[20] J. K. Park, *J. Chem. Phys*. **1997**, *107*, 6795; J. K. Park, *J. Chem. Phys*. **1998**, *109*, 9753.
[21] E. M. Evleth and E. Kassab, *Pure Appl. Chem*. **1988**, *60*, 209.
[22] E. Kassab and E. M. Evleth, *J. Am. Chem. Soc*. **1987**, *109*, 1653.
[23] J. Kaspar, V. H. Smith, Jr., and B.N. McMaster, *Chem. Phys*. **1985**, *96*, 81.
[24] M. Meot–Ner, *J. Am. Chem. Soc*. **1984**, *106*, 1257.
[25] H. Cardy, D. Liotard, A. Dargelos, and E. Poquet, *Chem. Phys*. **1983**, *77*, 287.
[26] S. Havriliak and H. F. King, *J. Am. Chem. Soc*. **1983**, *105*, 4.
[27] E. Broclawik, J. Mrozek, and V. H. Smith, Jr., *Chem. Phys*. **1982**, *66*, 417.
[28] D. L. Albritton, *At. Data Nucl. Data*, **1978**, *Tables 22*, 1.
[29] A. Pullman and A. M. Armbruster, *Chem. Phys. Lett*. **1975**, *36*, 558.
[30] W. A. Lathan, W. J. Hehre, L. A. Curtiss, and J. A. Pople, *J. Am. Chem. Soc*. **1971**, *93*, 6377.
[31] W. Strehl, H. Hartmann, K. Hensen, and W. Sarholz, *Theo. Chim. Acta*, **1970**, *18*, 290.
[32] R. S. Mulliken, *J. Chem. Phys*. **1933**, *1*, 492.
[33] H. J. Bernstein, *J. Am. Chem. Soc*. **1963**, *85*, 484.
[34] J. L. Magee, *Radiat. Res. Suppl*. **1964**, *4*, 20.

[35] T. J. Sworski, *J. Am. Chem. Soc.* **1964**, *86*, 5034; *J. Am. Chem. Soc.* **1955**, *77*, 4689.
[36] M. Kongshaug, H. B. Steen, and B. Cercek, *Nature Phys. Sci.* **1971**, *234*, 97.
[37] C. E. Melton and H. W. Joy, *J. Chem. Phys.* **1967**, *46*, 4275; *J. Chem. Phys.* **1968**, *48*, 5286.
[38] T. W. Martin and L. L. Swift, *J. Am. Chem. Soc.* **1971**, *93*, 2788.
[39] T. A. Claxton, I. S. Ginns, M. J. Godfrey, K. V. S. Rao, and M. C. R. Symons, *J. Chem. Soc. Faraday Trans. II*, 1973, *69*, 217.
[40] G. I. Gellene and R. F. Porter, *J. Chem. Phys.* **1984**, *81*, 5570.
[41] B. E. Turner, *Symp. Int. Astron. Union*, **1992**, *150*, 181.
[42] D. Bassi, M. De Paz, A. Pesce, and F. Tommasini, *Chem. Phys. Lett.* **1974**, *26*, 422.
[43] D. M. Bishop, *J. Chem. Phys.* **1968**, *48*, 5285.
[44] R. A. Gangi and R. F. W. Bader, *Chem. Phys. Lett.* **1971**, *11*, 216.
[45] W. A. Lathan, W. J. Hehre, L. A. Curtiss, and J. A. Pople, *J. Am. Chem. Soc.* **1971**, *93*, 6377.
[46] K. S. E. Niblaeus, B. O. Roos, and P. E. M. Siegbahn, *Chem. Phys.* **1977**, *25*, 207.
[47] S. Raynor and D. R. Herschbach, *J. Phys. Chem.* **1982**, *86*, 3592.
[48] I. Martin, P. Campo, and C. Lavin, *Int. J. Quantum Chem. Symp.* **1995**, *29*, 631.
[49] M. Luo and M. Jungen, *Chem. Phys. Lett.* **1999**, *241*, 297.
[50] M. E. Schwarz, *Chem. Phys. Lett.* **1976**, *40*, 1.
[51] J. K. Park, *Chem. Phys. Lett.* **1999**, *315*, 119; *Chem. Phys. Lett.* **2002**, *356*, 63.
[52] W. R. Wadt and N. W. Winter, *J. Chem. Phys.* **1977**, *67*, 3068.
[53] A. Mavridis and J. F. Harrison, *J. Chem. Soc. Faraday Trans.* **1982**, *78*, 447.
[54] M. Bettendorff, R. J. Buenker, S. D. Peyerimhoff, and J. Römelt, *Z. Phys. A*, **1982**, *304*, 125.
[55] P. Botschwina, in Molecular Ions: Geometrical and Electronic Structures, edited by J. Berkowitz and K. Groeneveld, Plenum, New York, 1983.
[56] H. F. Schaefer III, *J. Phys, Chem.* **1985**, *89*, 5336.
[57] J. C. Polanyi, M. G. Prisant, and J. S. Wright, *J. Phys, Chem.* **1987**, *91*, 4727.
[58] I. D. Petsalakis, G. Theodorakopoulos, J. S. Wright, and I. P. Hamilton, *J. Chem. Phys.* **1988**, *88*. 7633.
[59] I. D. Petsalakis, G. Theodorakopoulos, J. S. Wright, and I. P. Hamilton, *J. Chem. Phys.* **1988**, *89*. 6841.
[60] M. Gutowski and J. Simons, *J. Chem. Phys.* **1990**, *93*, 2546.
[61] F. Chen and E. R. Davidson, *J. Phys, Chem.* **2001**, *105*, 10915.
[62] M. J. Frisch, J. S. Binkley, and H. F. Schaefer III, *J. Chem. Phys.* **1984**, *81*, 1882.
[63] A. B. Raksit, S.–J. Jeon, and R. F. Porter, *J. Phys, Chem.* **1986**, *90*, 2298.
[64] E. Schäfer and R. J. Saykally, *J. Chem. Phys.* **1984**, *81*, 4189.
[65] S. Huzinaga, J. Andzelm, M. Klobukowski, E. Radzio–Andzelm, Y. Sakai, and H. Tatewaki, *Physical Science Data*, Gaussian basis sets for molecular calculations, Vol. 16, Elsevier, Amsterdam, 1984.
[66] F. B. Duijneveldt, *IBM Research Report NO. R J*, **1971**, 945.
[67] K. Hasimoto and Y. Osamura, *J. Chem. Phys.* **1991**, *95*, 1121.
[68] H. Partridge, C. W. Bauschlicher, Jr., and S. R. Langhoff, *Theo. Chim. Acta*, **1990**, *77*, 323.
[69] R. Poirier, R. Kari, and I. G. Csizmadia, *Physical Science Data*, Handbook of Gaussian basis sets, Vol. 24, Elsevier, Amsterdam, 1984.
[70] A. Skerbele and E. N. Lassettre, *J. Chem. Phys.* **1965**, *42*, 395.
[71] D. H. Aue and M. T. Bowers, *Gas Phase Ion Chemistry II*, Eds. M. T. Bowers, Academic Press, New York, 1979, pp.1.
[72] R. Runau, S. D. Peyerimhoff, and R. J. Buenker, *J. Mol. Spectrosc.* **1977**, *68*, 253.
[73] R. L. Graham, J. T. Golab, and D. L. Yeager, *J. Chem. Phys.* **1988**, *88*, 2572.
[74] J. A. Pople and L. A. Curtis, *J. Phys. Chem.* **1987**, *91*, 155.
[75] S. J. Dunlavey, J. N. Dyke, N. Jonathan, and A. Morris, *Mol. Phys.* **1980**, *39*, 1121; J. N. Dyke, N. Jonathan, and A. Morris, *Int. Rev. Phys. Chem.* **1982**, *2*, 3.
[76] S. A. Pope, I. H. Hillier, and M. J. Guest, *Faraday Symp. Chem. Soc.* **1984**, *19*, 109.
[77] S. T. Gibson, J. P. Greene, and J. Berkowitz, *J. Chem. Phys.* **1985**, *83*, 4319.
[78] R. Vetter, L. Zülicke, A. Koch, E. F. van Dishoeck, and S. D. Peyerimhoff, *J. Chem. Phys.* **1996**, *104*, 5558.
[79] H. Biehl, G. Schönnenbeck, F. Stuhl, and V. Staemmler, *J. Chem. Phys.* **1994**, *101*, 3819.
[80] R. P. Saxon, B. H. Lengsfield III, and B. Liu, *J. Chem. Phys.* **1983**, *78*, 312.
[81] S. D. Peyerimhoff and R. J. Buenker, *Can. J. Chem.* **1979**, *57*, 3182.
[82] L. A. Curtiss, K. Raghavachari, G. W. Trucks, and J. A. Pople, *J. Phys. Chem.* **1991**, *94*, 7221.
[83] H. H. Bueker and E. Uggerud, *J. Phys. Chem.* **1995**, *99*, 5945.
[84] C. Y. Ng, D. J. Trevor, P. W. Tiedemann, S. T. Ceyer, P. L. Kronebusch, B. H. Mahan, and Y. T. Lee, *J. Phys. Chem.* **1977**, *67*, 4235.
[85] G. Herzberg, *Moleclar Spectra and Moleclar Structure III*. Electronic Spectra and Electronic Structure of Polyatomic Molecules, Van Nostrand, New York, 1966.

[86] H. Sun, M. G. Sheppard, and K. F. Freed, *J. Chem. Phys.* **1981**, *74*, 6842.
[87] A. Streitwieser, Jr. and R. W. Taft, *Progress in Physical Organic Chemistry*, **1974**, *11*, 175.
[88] P. E. Cade and W. M. Huo, *J. Chem. Phys.* **1967**, *47*, 614.
[89] P. E. Cade, *Proc. Phys. Soc.* **1967**, *91*, 842.
[90] R. D. Vivie, C. M. Marian, and S. D. Peyerimhoff, *Mol. Phys.* **1988**, *63*, 3.
[91] A. D. Esposti and H.–J.Werner, *J. Chem. Phys.* **1990**, *93*, 3351.
[92] P. J. Bruna, G. Hirsch, R. J. Buenker, and S. D. Peyerimhoff, *Molecular Ions*, *NATO*, *ASI Series*, 1984, pp. 309.
[93] G. Herzberg, *Molecular Spectra and Molecular Structure IV*, Constants of Diatomic Molecules; Spectra of Diatomic Molecules, Van Nostrand Reinhold, New York, 1979.
[94] E. de Beer, E. H. Kim, D. M. Neumark, R. F. Gunion, and W. C. Lineberger, *J. Phys. Chem.* **1995**, *99*, 13627.
[95] R. L. Kelly and D. E. Harrison, Jr., *Atomic Data* **1971**, *3*, 177.

Biographies

Jong Keun Park is assistant professor of chemistry education at the Gyeongsang National University. After obtaining a Ph.D. degree in physical chemistry of "Applications of Effective Valence Shell Hamiltonian to the Valence States of NH, SiH, PH, and SH" from the Pusan National University, Dr. Park undertook postdoctoral research with Professor Iwata at the Institute of Molecular Science, Japan. More recently, Dr. Park has collaborated on projects with Professor Lee at Pusan National University.